A COMPUTATIONALLY EFFICIENT MODELLING OF LAMINAR SEPARATION BUBBLES

SEMI-ANNUAL STATUS REPORT

June 1988–January 1989

for

NASA Grant NAG-1-778

Paolo Dini
and
Mark D. Maughmer

Department of Aerospace Engineering
The Pennsylvania State University
University Park, PA 16802

February 1989

TABLE OF CONTENTS

NOMENCLATURE

b = width of separated shear layer
c = airfoil chord
c_d = section drag coefficient
c_f = skin-friction coefficient
c_ℓ = section lift coefficient
c_m = section moment coefficient about quarter-chord point
h = distance of separated shear layer from airfoil surface
ℓ_1 = laminar length of the bubble
ℓ_2 = turbulent length of the bubble
n = linear stability theory amplification factor
s = streamwise coordinate from the stagnation point
u = streamwise velocity inside the boundary layer
y = normal distance from the surface
C_D = dissipation coefficient
C_p = pressure coefficient
C_{δ_2} = momentum thickness growth factor for free shear layer
DL = step size for shear layer Runge-Kutta integration
DU = inviscid velocity decrease as $\ell_1 \rightarrow \infty$
G = amplitude of Coles's wake function in Green's profiles
H_{12} = boundary-layer shape factor, (δ_1/δ_2)
H_{32} = boundary-layer shape factor, (δ_3/δ_2)
P = Gaster's pressure gradient parameter
R = chord Reynolds number, $(U_\infty c/\nu)$
R_{ℓ_1} = laminar length Reynolds number, $(U_S \ell_1/\nu)$
R_{δ_2} = momentum thickness Reynolds number, $(U\delta_2/\nu)$
SF = scaling factor to match pressure gradients at laminar separation
U = velocity at the edge of the boundary layer/inviscid velocity
U_∞ = freestream velocity
XB = distance from s_R to first airfoil coordinate after s_R
XU = laminar fraction within one boundary-layer step
α = angle of attack relative to the chord line
δ_1 = boundary-layer displacement thickness
δ_2 = boundary-layer momentum thickness
δ_3 = boundary-layer kinetic energy thickness
ν = kinematic viscosity of air
ξ = dimensionless streamwise coordinate inside the bubble

Subscripts:

S = laminar separation point
R = turbulent reattachment point
T = transition point
TE = trailing edge
TS = turbulent separation

I. SUMMARY

The present effort to develop a computationally efficient model for laminar separation bubbles began approximately a year and a half ago. At the present stage, the development of laminar separation bubbles in low-turbulence flow over smooth airfoils has been found primarily dependent on three physical factors: chord Reynolds number, boundary-layer development upstream of laminar separation, and pressure recovery gradient along the bubble. These variables can be conveniently grouped into a single dimensionless quantity, Gaster's[1] pressure gradient parameter. A general, semi-empirical bubble model has been developed and incorporated into the airfoil design and analysis program of Eppler and Somers.[2] The essential feature of this model is the linking of transition to the development of the separated laminar shear layer which, in turn, depends on local and global flow characteristics through an iteration on Gaster's parameter. This has been achieved with a minimum computational penalty over the existing program.

In its present form the model still requires some amount of refinement. The data base used to develop the transition criterion is very limited and mainly from one facility. The agreement of the predicted pressure distribution in the laminar part of the bubble with available measurements has allowed the calculation of the development of the shear layer in the direct mode. The Stewartson[3] profiles upon which the closure relationships between the integral boundary-layer parameters used in the present model are based, however, may be poor approximations for the velocity profiles in the laminar part of the bubble. As a consequence, the model is at present unable to sufficiently resolve the transition length as a function of angle of attack.

Using Green's[4] two-parameter family of reversed profiles, Fitzgerald and Mueller[5] have obtained good agreement with LDV measurements inside the bubble. Closure relationships based on these profiles have therefore been developed and compared with the corresponding relationships based on the Stewartson profiles. It is hoped that the greater flexibility of the Green's profiles, afforded by their dependence on an additional parameter, will enable

the model to follow more closely the behavior of the bubble in differing flow conditions. Once the transition location and growth of δ_2 in the laminar part of the bubble have been modelled accurately and with sufficient generality, the problem of predicting the growth in δ_2 in the turbulent part can be addressed with confidence that it will lead to accurate drag predictions.

II. RESEARCH DESCRIPTION

The goal of this research is to accurately predict the characteristics of the laminar separation bubble and its effects on airfoil performance. Toward this end, a computational model of the separation bubble has been developed and incorporated into the Eppler and Somers[2] airfoil design and analysis program. Thus far, the focus of the research has been limited to the development of a model which can accurately predict situations in which the interaction between the bubble and the inviscid velocity distribution is weak, the so-called short bubble. In this section, a summary of the research performed in the past nine months is presented. The bubble model in its present form is then described. Lastly, the performance of this model in predicting bubble characteristics is shown for a few cases.

Summary of Research

As described in Ref. 6, the first activity in the development of a short-bubble model was to insert the model of Horton,[7] modified according to suggestions by Roberts,[8] into the Eppler and Somers program. Not unexpectedly, the performance of this model was found unsatisfactory. As shown in Fig. 1, the aerodynamic performance of the Eppler 387 airfoil predicted by the original version of the Eppler and Somers program, where the analysis method switches from the laminar to the turbulent boundary-layer equations at laminar separation, does better than the modified version when compared with the experimental data of McGhee et al.[9] This is only partly due to an inaccurate transition prediction since, as shown in Fig. 2, Schmidt's[10] empirical transition criterion does capture the lowest-order behavior of the bubble. The large region of separation predicted in the mid-c_ℓ range (Fig. 1) is not observed experimentally. It is thought to be a result of predicting too large of an increase in δ_2 along the bubble.

As discussed in Ref. 6, the excessive increase in δ_2 is a consequence of the shape assumed for the recovery pressure distribution in the turbulent part of the bubble. More specifically, if the boundary-layer assumptions and Horton's assumption of a constant

(C_D/H_{32}) are valid, then the increment in momentum thickness between transition and reattachment is directly proportional to the area under the pressure recovery curve between these two points. In Fig. 3, the inviscid pressure distribution for the Eppler 387 airfoil at $\alpha = 0^0$ is shown together with two possible bubble geometries. For a fixed transition point, it can be seen how the area under the Stratford pressure distribution, originally proposed in this context by van Ingen,[11] is less than that under the linear distribution assumed by Horton. That the area is less is also a consequence of the greater steepness of the Stratford curve as compared to the locus of possible reattachment points used by Horton, shown as a dotted line. The more favorable correlation of the Stratford recovery with the bursting behavior of bubbles, as discussed by van Ingen and Boermans,[12] provides another reason for its use against Horton's. The Stratford curve has been included in the program and is used to numerically integrate the energy integral equation to obtain the increment in δ_2. The effect of this modification on the drag polar is shown in Fig. 4. The unrealistic separation is greatly reduced. The predicted bubble geometry is not very different from that of Fig. 2 except for a slight shortening of the bubble.

Inviscid vs. Experimental Pressure Distribution

At this point, it was thought that part of the cause for the discrepancy in drag prediction could be the inability of the present model to account for viscous/inviscid interaction. Therefore, before the influence of the separation bubble on the drag could be investigated, it was necessary to isolate this from the inability of the boundary-layer method to account for the effects of viscosity on the pressure distribution. This was accomplished by employing experimental pressure distributions, also from Ref. 9, as input to the boundary-layer analysis.

The effects of using the experimental pressure distribution (the "inviscid" behavior in the bubble region approximated by joining a straight line between the separation and reattachment points) for the conditions of Fig. 4 are shown in Fig. 5. The drag is underpredicted at the lower angles of attack and the region of turbulent separated flow is moved to lower c_ℓ's. In Fig. 6, the laminar separation point is followed more closely than

it was with the inviscid distribution and, therefore, the overall gross behavior of the bubble is reproduced better. It is particularly interesting that the transition correlation, although resulting in a decreasing bubble length, does not reproduce the gradual vanishing into natural transition with increasing angle of attack. Thus, in addition to Schmidt's transition correlation, that of O'Meara and Mueller[13] and that of Horton,[7] both also described in Ref. 6, were tried. Neither of these, however, improved the prediction.

In order to determine the importance of bubble length in predicting the drag, the experimental bubble lengths were matched at all angles of attack by artificially adjusting the transition points. In this case, the drag was underpredicted at the higher angles of attack. These numerical experiments led to two important conclusions. First, as is apparent by examination of the experimental pressure distributions presented in Figs. 7-9, Horton's assumption of a constant pressure in the laminar part of the bubble, while possibly a good assumption for short leading-edge bubbles in high Reynolds number flows, is inadequate for the longer mid-chord bubbles. For this reason, van Ingen and Boermans's[12] velocity distribution in the laminar part of the bubble was included in the model,

$$\frac{U}{U_S} = .978 + .022\exp(-4.454\xi - 2.5\xi^2) \tag{1}$$

where

$$\xi = \frac{s - s_S}{(R_{\delta_2})_S(\delta_2)_S} \tag{2}$$

Second, even at low Reynolds numbers, it does not seem necessary to employ potential flow/boundary layer iteration. Although there are differences between the inviscid and experimental pressure distributions at a given angle of attack, these are largely due to the fact that the influence of the boundary layer on the zero-lift angle of attack has not been taken into account. Since aerodynamic characteristics are usually compared at the same c_ℓ rather than at the same α, however, the constant difference in angle of attack between the inviscid and experimental lifts poses no obstacles to comparing drag predictions obtained with the inviscid pressure distribution to the experimental drag polar. In the non-linear c_ℓ-range, of course, such a comparison cannot be made without considering the effect of the

turbulent separated region progressing upstream from the trailing edge. Eppler's correction to the aerodynamic properties in the presence of turbulent trailing-edge separation is quite reliable and has been used extensively in the past. To analyze weakly interacting bubbles, therefore, use of the inviscid pressure distribution should provide satisfactory results even at very low Reynolds numbers.

Reattachment Region

In the results presented above, turbulent separation is erroneously predicted at the higher lift coefficients. In addition to an overprediction of the increase in δ_2 along the bubble, this may be the result of a lack of generality with the turbulent boundary-layer method used in the Eppler and Somers program. More specifically, the region downstream of reattachment is characterized by a relaxing turbulent boundary layer. This is the most difficult kind of boundary layer to analyze in that it is highly nonequilibrium and history effects play a dominant role. The analysis method used in the program is based on empirical *equilibrium* relationships between the integral parameters and cannot, therefore, account for any turbulence lag.

As shown in Ref. 4 for a turbulent shear layer forming a free stagnation point behind a base, some pressure recovery occurs downstream of the stagnation point. The same behavior is observed in a reattaching laminar separation bubble. In the measurements of Ref. 9, the intersection of the pressure recovery distribution in the turbulent part of the bubble with the inviscid pressure distribution occurs downstream of the reattachment location actually observed with oil flow. Furthermore, as Fig. 7 shows, the pressure distribution exhibits a characteristic "undershoot," or additional rise over the inviscid value, for a distance of 10% of chordlength or more downstream of reattachment. This may be indicative of the extent of the relaxing region. To explore the effect of such a relaxing boundary layer, the method of Felsch, Geropp, and Waltz[14] was implemented as it incorporates non-equilibrium contributions in empirical relationships that are very similar to those of Eppler. This had been previously done by Miley.[15] As shown in Fig. 10, a reasonably good prediction is obtained with this method. Before a complete assessment

of this method can be made, however, it is first necessary to establish the accuracy of the momentum-thickness growth prediction within the bubble.

As the bubble model does not account for any pressure interaction in the reattachment region, a method more sophisticated than that of Eppler may not be necessary. It will depend on the impact of the relaxing region on the growth of δ_2. If the inviscid pressure distribution is employed downstream of its intersection with the Stratford recovery, however, it seems almost certain that boundary-layer parameter values different from those actually measured at reattachment will be necessary to start the turbulent calculations, regardless of the boundary-layer method used. An indication for what these values should be is provided by Eppler's "bubble analog," used in the unmodified version of the program to monitor whether or not a bubble might cause a significant drag increase. It is based on the pressure increase over which H_{32}, as calculated from the turbulent boundary-layer method, reaches the value 1.60 from the point of laminar separation, $(H_{32})_S = 1.515095$. Since a value of 1.58 marks the upper limit for possible turbulent separation, according to Eppler,[16] in the present version of the bubble model a similar value is used at the "reattachment" point, $(H_{32})_R = 1.57$. As $(\delta_2)_R$ is calculated by the bubble model, the turbulent closure relationships can be used to obtain the values of the other boundary-layer parameters at reattachment, $(H_{12})_R$, $(c_f)_R$, and $(C_D)_R$.

Figs. 11 and 12 show the predictions obtained using Eppler's turbulent boundary-layer method from the reattachment point as predicted by the bubble model. Each of these is compared with the corresponding predictions assuming transition at laminar separation. By comparing Fig. 12 to Fig. 4, the effects of the changes to the bubble model discussed above can be seen clearly. Using Eq. (1) instead of Horton's constant pressure plateau has decreased the value of U_T. As a consequence, the increment in momentum thickness in the turbulent part of the bubble and, therefore, the drag predicted, are smaller. A smaller value of $(\delta_2)_R$ and use of $(H_{32})_R = 1.57$ instead of 1.51 have eliminated the premature turbulent separation. The decrease in bubble length with angle of attack causes the drag increment due to the bubble to decrease correspondingly. As with the method of Ref. 14,

no conclusions can be reached about Eppler's method until the accuracy of the momentum thickness growth prediction along the bubble can be relied on for any bubble geometry. In any case, during the development of the bubble model Eppler's turbulent boundary-layer correlations have been used.

Having obtained a first estimate for the adequacy of using the inviscid pressure distribution and for the accuracy of the momentum-thickness growth prediction within a given bubble geometry, the prediction of the geometry itself appears to be the most important aspect of the bubble problem. Predicting bubble size is strongly dependent on predicting transition.

Transition

The starting point in the development of a general and accurate transition criterion was to compare Eppler's empirical criterion for attached boundary layers to the e^n method.[17,18] The development of the amplification factor, n, can be expressed as a function of variables similar to the ones used by Eppler to describe the boundary-layer development, namely R_{δ_2} and H_{12}. The success of both methods suggests that Eppler's transition curve should lie quite close to the linear stability curve corresponding to a value of $n = 10$, say, when the two methods are plotted together in terms of these variables. In addition, as the e^n method is easily extendable to separated boundary layers, such as the family of reversed Falkner-Skan, or Stewartson,[3] profiles, it was hoped to extrapolate Eppler's criterion to separated flow by following the corresponding n-contour. Conversely, as the best value of n for use in separation bubbles is still being debated in the literature,[19] it was thought that such an extrapolation might help resolve this issue.

Rather than developing the function $n(R_{\delta_2}, H_{12})$, it was chosen to use that given by Drela.[20] Fig. 13 shows contours of constant n, for $0 \leq n \leq 63$, as well as Eppler's transition criterion, for $2.24 < H_{12} < 4$, on the same R_{δ_2} vs. H_{12} plot. H_{12} is plotted as a reversed axis for ease of comparison with corresponding values of H_{32}. The disagreement between the $n = 9$ curve and that of the Eppler criterion is surprising. The only region where the two criteria are close is near zero pressure gradient. The absence of a clear correlation

prompted a search for experimental values of R_{δ_2} and H_{12} measured at transition inside separation bubbles. Only a few points have been found, mostly from the measurements of Brendel and Mueller.[21]

As shown in Fig. 13, a first attempt of obtaining a transition criterion for separated boundary layers is provided by extending Eppler's transition criterion from $H_{12} = 4$ to a much lower value of R_{δ_2} at $H_{12} = 20$. Since the data from Mueller's group comes from a wind tunnel, Eppler's criterion was extrapolated directly as it is believed to better reflect the transition locus for free flight. The high values of n apparently necessary to reach the extrapolation to separated flows of Eppler's criterion simply reflect the limitations of the e^n method. It is generally accepted that linear stability theory correctly models the transition process for approximately 70% of the distance between neutral stability ($n = 0$) and fully turbulent flow. The actual "transition region," however, is usually defined as the region between the first appearance of turbulent spots and fully turbulent flow.[24] Thus, a value close to $n = 10$ can be regarded as marking the boundary between the linear amplification region and transition onset in accordance with this definition. While the value of n at the end of the transition region is still probably close to 15 or 20, and *not* 63, this value is reached through a non-linear transition process which is not modelled by linear stability theory. In fact, in practice an intermittency function is usually employed from the point marking the end of the linear amplification region in order to mimick the non-linear transition process before the fully turbulent calculations begin.

Eppler's curve and its extrapolation, on the other hand, are closer to the end of the whole transition region and the beginning of the full turbulent calculations. As explained in Ref. 25, for the transition of attached boundary layers the turbulent calculations are commenced using the laminar boundary-layer parameter values at the transition point. The distance it takes for the parameters to reach the turbulent values accounts to some extent for a "transition region." As the change in parameter values is very quick, however, this distance is much shorter than the one over which an intermittency function is usually used. As the Reynolds number decreases, transition occurs in increasingly adverse pressure

gradients and over a longer region of the airfoil surface. Thus, the discrepancy between Eppler's transition criterion and the e^9 curve in Fig. 13 increases until laminar separation precedes transition. The criterion for separated boundary layers shown here is therefore considered a physically plausible extension of Eppler's criterion. Although the transition criterion shown does not follow the behavior of the constant n contours, it has thus far given the best correlation with experimental bubble lengths when used in conjunction with the bubble model that will now be described.

Laminar Separation Bubble Model

Encouraging as the insight gained from a study of the transition problem may be, in order to utilize a criterion such as the one shown in Fig. 13, it is necessary to calculate the development of the separated laminar boundary layer. The fastest known way to do this is by means of a global displacement-thickness iteration algorithm coupled with inverse boundary-layer formulations for the laminar and turbulent parts of the bubble. While such an algorithm is certainly much faster than a finite-difference approach, an even faster means is highly desirable for use in a design code such as the one of Eppler and Somers. Thus, an approximation to an interaction method has been attempted and is currently under development.

Initial Bubble Model

Van Ingen and Boermans's velocity distribution in the laminar part of the bubble, Eq. (1), matches the measured pressure distribution quite well, in some cases. This distribution, unlike Horton's constant-pressure plateau, allows a slight pressure recovery after laminar separation, quickly approaching a limiting value. Using detailed pressure distributions in the bubble region available from recent wind-tunnel tests of the NASA NLF(1)-1015 airfoil in the NASA-Langley Low-Turbulence Pressure Tunnel, the accuracy of Eq. (1) was checked for several different conditions. It was found that, as the pressure gradient along the bubble decreases, the pressure distribution tends to fall below van Ingen's curve while, as the pressure gradient steepens, it becomes flatter, closer to Horton's

approximation and above van Ingen's curve. It is therefore postulated that Eq. (1) can be improved by relaxing the amount of pressure recovery between separation and transition,

$$\frac{U}{U_S} = (1 - DU) + DU \exp(-4.454\xi - 2.5\xi^2) \tag{3}$$

The steeper the pressure gradient along the bubble, the smaller the value DU.

The behavior of the velocity distribution as described above is consistent with an inviscid velocity calculated over an ever thickening displacement surface in a steepening adverse gradient. A first approximation to the development of the laminar shear layer that would reflect this behavior was therefore attempted. The growth in δ_2 is obtained from a generalization of Schmidt's[10] self-similar free shear layer solution,

$$\frac{\delta_2}{(\delta_2)_S} = \sqrt{1 + C_{\delta_2}\xi} \tag{4}$$

where C_{δ_2} is also a function of the pressure gradient along the bubble. Assuming that skin friction is negligible, the variation in H_{12} is obtained from the momentum integral equation,

$$H_{12} = -2 - \frac{U}{\delta_2}\left[\frac{d\delta_2}{ds} \Big/ \frac{dU}{ds}\right] \tag{5}$$

A check for transition is made at each downstream increment from separation by calculating R_{δ_2} and by comparing it to the transition criterion shown in Fig. 13,

$$\log_{10}[(R_{\delta_2})_T] \geq 2.7321 + .05774H_{12} - .007217(H_{12})^2 \qquad 4 < H_{12} < 20 \tag{6}$$

Since the exact functional dependence of DU and C_{δ_2} on the dimensionless pressure gradient between laminar separation and turbulent reattachment is not known, many candidate functions were tested. Although in some cases excellent agreement between the calculated and the measured drag polars was obtained for one airfoil, the bubble model so configured lacks generality.

Pressure Distribution in the Laminar Part of the Bubble

By comparing measured bubble geometries to the ones predicted with the above model, it was realized that the boundary-layer development upstream of separation may have an

even stronger influence than was taken into account. Thus, as Gaster's[1] pressure gradient parameter includes the value of momentum thickness at separation,

$$P = \frac{(\delta_2)_S^2}{\nu} \frac{\Delta U}{\Delta s} \tag{7}$$

it was thought that this might be a better independent parameter than simply the average pressure gradient along the bubble,

$$\frac{\Delta(U/U_\infty)}{\Delta(s/c)} = \frac{(U_S - U_R)/U_\infty}{(s_S - s_R)/c} \tag{8}$$

In dimensionless variables P becomes

$$P = R \left[\frac{(\delta_2)_S}{c}\right]^2 \frac{\Delta(U/U_\infty)}{\Delta(s/c)} \tag{9}$$

and embodies all three factors on which the bubble depends. Having specified this independent parameter, it is necessary to determine whether a unique relationship links DU and P. To this end, these variables have been extracted directly from the experimental pressure distributions of the NLF(1)-1015 and the E387 airfoils. As Fig. 14 shows, the collapse of the points around a unique relationship is acceptable. The width of the scatter is of the same order of magnitude as that caused by reading error. The solid line is a quadratic least-squares fit that has been included in the model,

$$DU = 0.0609691 + 0.304819P + 0.507176P^2 \tag{10}$$

Van Ingen and Boermans's[12] original value of $DU = 0.022$ falls in the middle of the variation in DU shown in Fig. 14. In the near future it is planned to utilize available experimental data, such as that of Refs. 26, 27, and 28, to confirm and refine this functional dependence.

When the velocity distribution defined by Eqs. (3) and (10) is used in conjunction with the approximate development of the separated laminar shear layer described above, large discontinuities in the boundary-layer parameters appear at the point of laminar separation. Upon examination of the bubble velocity distribution near the point of laminar separation,

unlike in the experimental distribution, it was noticed that a discontinuity in the velocity gradient was present. In order to match the gradients at laminar separation, a further unknown is therefore introduced in the original velocity distribution of van Ingen and Boermans's, Eq. (1). Specifically, the product $[(R_{\delta_2})_S(\delta_2)_S]$ in Eq. (2) serves simply as a scaling factor between the physical variable s and the universal dimensionless variable ξ. Thus, the scaling factor is now solved for as that which yields a velocity distribution in the laminar part of the bubble whose gradient is continuous with the gradient of the inviscid velocity distribution at separation. By forward-differencing the velocity gradient at separation, the boundary-layer edge velocity a small distance DL downstream of separation is simply

$$U_{DL} = U_S + DL\left(\frac{dU}{ds}\right)_S \tag{11}$$

For this value of the velocity, Eq. (3) becomes

$$\frac{U_{DL}}{U_S} = (1 - DU) + DU \exp\left[-4.545\frac{DL}{SF} - 2.5\left(\frac{DL}{SF}\right)^2\right] \tag{12}$$

Eliminating U_{DL} between these two equations leads to an explicit expression for the scaling factor,

$$SF = -\frac{1}{2}\left\{\frac{4.545DL}{\log\left[1 + \frac{DL}{U_S DU}\left(\frac{dU}{ds}\right)_S\right]}\right\} + \frac{1}{2}\sqrt{\left\{\frac{4.545DL}{\log\left[1 + \frac{DL}{U_S DU}\left(\frac{dU}{ds}\right)_S\right]}\right\}^2 - \frac{10DL^2}{\log\left[1 + \frac{DL}{U_S DU}\left(\frac{dU}{ds}\right)_S\right]}} \tag{13}$$

This factor is of the same order of magnitude as $[(R_{\delta_2})_S(\delta_2)_S]$.

Present Bubble Model

Eppler's boundary-layer analysis method employs two coupled governing ordinary differential equations, the momentum and energy integral equations, together with appropriate closure relations.[25] As discussed by Drela,[20] contrary to simpler, one-equation methods such as that of Thwaites, in two-equation methods the shape factor is not uniquely related

to the pressure gradient parameter. This allows methods such as Eppler's and Drela's to accurately analyze the non-similar boundary-layer developments characteristic of aerodynamic flows, provided that the assumed family of velocity profiles approximates the actual flow reasonably well. Since the discontinuities in boundary-layer parameters at laminar separation did not disappear after matching velocity gradients, it was decided to implement the same Runge-Kutta method used by Eppler to analyze attached boundary layers, together with the closure relationships based on the Stewartson profiles developed by Drela, to analyze the laminar part of the bubble. Instead of implementing this boundary-layer method in the inverse mode as it is usually done, however, the generality provided by the two-parameter family of velocity distributions suggests that it might be used in the direct mode.

In the present version of the bubble model, the development of the separated laminar shear layer is calculated exactly, within the approximation of the pressure distribution and of the assumed Stewartson[3] profiles. Since δ_2 and δ_3 are obtained directly from the governing equations,

$$\frac{d\delta_2}{ds} = \frac{c_f}{2} - (H_{12}+2)\frac{\delta_2}{U}\frac{dU}{ds} \tag{14}$$

$$\frac{d\delta_3}{ds} = C_D - 3\frac{\delta_3}{U}\frac{dU}{ds} \tag{15}$$

the transition criterion is expressed in terms of R_{δ_2} as a function of H_{32}, instead of H_{12},

$$\log_{10}[(R_{\delta_2})_T] \geq -30.936 + 44.797 H_{32} - 14.784(H_{32})^2 \tag{16}$$

This criterion is similar to Eq. (6) and is very preliminary. Once transition is detected, a Stratford pressure distribution joins (s_T, U_T) to (s_R, U_R), on the inviscid pressure distribution. The increment in δ_2 in the turbulent part of the bubble is found by using the Stratford curve in the integrated form of the energy integral equation as previously discussed.

To account for the pressure gradient the bubble is actually trying to overcome, the model is closed by introducing a simple local iteration algorithm. The pressure gradient

at laminar separation is used to obtain an initial guess at P, from which an initial velocity distribution, shear layer development, and transition and reattachment points are obtained. The resulting pressure gradient along the bubble, $\frac{\Delta(U/U_\infty)}{\Delta(s/c)}$, is used to obtain a second estimate at P and the bubble calculations repeated. The third and subsequent iterates are obtained by means of a relaxed Newton's method operating on the *difference* between subsequent pressure gradients. The procedure converges very quickly to a pressure gradient along the bubble exactly equal to the one used to calculate the development of the laminar part. In drag polar analyses, it has been found helpful and efficient to utilize the converged value of pressure gradient at one angle of attack as the initial guess for the subsequent angle of attack.

Preliminary Results

The laminar separation bubble model described above promises to be very general and very accurate. In fact, it is formulated in terms of the governing equations and of very general and flexible functions whose dependence on local and global flow characteristics has been determined. The transition criterion, which controls the size of the bubble, is inextricably linked to the development of the separated laminar boundary layer and to conditions at separation such that, as $(R_{\delta_2})_S$ increases, the difference $[(H_{32})_T - (H_{32})_S]$ approaches zero. The development of the separated laminar boundary layer, in turn, is driven by a velocity distribution function which is completely determined by Gaster's pressure gradient parameter and by the velocity gradient at laminar separation. This version of the bubble model, however, is limited in that its accuracy depends on the accuracy with which the family of reversed profiles used in deriving the closure relationships $H_{12}(H_{32})$, $c_f(H_{32}, R_{\delta_2})$, and $C_D(H_{32}, R_{\delta_2})$ reproduces the actual flow. As discussed by Fitzgerald and Mueller,[5] LDV measurements inside the bubble show velocity profiles that are quite different from the Stewartson profiles, whose use in the present model could therefore explain the difficulties encountered. This problem is currently being addressed.

The most convenient way to illustrate how the transition criterion, Eq. (16), is used

is by plotting it together with the shear layer development on the same plot that Eppler uses to describe the boundary-layer development. Since H_{32} and R_{δ_2} are calculated at each point along the boundary layer, by connecting subsequent (H_{32}, R_{δ_2})-pairs on a plot whose axes measure the variation of these two variables, the boundary-layer development from the stagnation point to the trailing edge can be described in a very concise way. In addition, since all the separation and transition criteria are expressed in terms of these two variables, such a plot is especially useful. Fig. 15 shows the boundary-layer development for the E387 airfoil at $\alpha = -2.3°$ and $R = 300,000$. The transition criteria and the bondary-layer separation conditions are indicated on the plot. While the actual development of the shear layer between separation and transition is plotted, a straight line joins transition to reattachment. The upper surface has a mid-chord bubble which causes a moderate increase in R_{δ_2}, while the lower surface has a short leading-edge bubble. The intersection of the curve defining the development of the laminar part of the bubble with the transition criterion occurs outside of the range of the plot.

Fig. 16 shows the pressure distribution corresponding to the boundary-layer development of Fig. 15. The close agreement with the experimental pressure distribution at $\alpha = -2°$ shows how the shift in zero-lift angle should not be regarded as strong viscous/inviscid interaction. The bubbles sizes, shapes, and locations are matched quite well. Fig. 17 shows the complete viscous analysis summary for the same angle of attack. To provide a better feel for the physical behavior of the bubble, the same graph of Fig. 15 is shown together with distributions of boundary-layer properties plotted as functions of arc length. The main shortcoming of the present model can be seen in the distribution of momentum thickness; its growth in the laminar part of the bubble is smaller than the resolution of the plotter, such that a horizontal line is shown. This prediction is believed erroneous. As all the boundary-layer variables are coupled, although the governing momentum and energy integral equations are believed correct, the wrong closure relations would cause the free shear layer development to be in error. As a result. the transition location may be wrong. In fact, the present model does not predict the gradual vanishing

of the bubble into natural transition as the pressure gradient increases as is observed in the experiments.

As an assessment of the generality of the present model, the NLF(1)-1015 airfoil was analyzed at $R = 500,000$. This airfoil is particularly difficult to analyze by any method due to the strong trailing-edge viscous/inviscid interaction induced by the large aft-loading. Such interaction causes a marked decrease in the aft-loading such that it is impossible, unlike for the E387, to find an angle of attack at which the experimental and inviscid pressure distributions correspond. Another consequence of this is that the lower surface bubble has a greater difficulty reattaching to the inviscid pressure distribution than in the actual flow. By adjusting the transition criterion, it is possible to make the lower surface reattach; however, although the transition prediction is not yet reliable for the reasons discussed above, it was desired to use exactly the same bubble model as for the E387. Therefore, rather than altering the transition criterion, the experimental pressure distribution was used to calculate the boundary-layer development. Fig. 18 shows this experimental pressure distribution, at $\alpha = 2°$, together with the inviscid at $\alpha = 1°$. The effect of the strong trailing-edge interaction is clearly visible. If the mismatch in the location of laminar separation is taken into account, the shape of the pressure distribution in the laminar part of the bubble is predicted quite well. Fig. 19 shows the boundary-layer development for this case.

III. RESEARCH PLANNED

Coupling the various parts of the bubble model and "anchoring" the pressure distribution in the laminar part to local flow characteristics has made the model quite general. The weakness of such a formulation, however, is that if one part of the model is not right everything else is affected. Thus, before further calibration of the model can proceed, a better family than the Stewartson profiles must be utilized to develop alternate closure relations to the ones presently used in calculating the development of the separated laminar shear layer.

Fitzgerald and Mueller[5] have obtained good agreement between their measurements and the two-parameter profile family originally developed by Green[4] for the turbulent reversed profiles in a reattaching shear layer downstream of a base. As shown in Fig. 20, the two parameters are linked to the geometrical characteristics of the profiles. (h/b) is the ratio of the distance of the shear layer from the centerline of the wake to the width of the shear layer and G is the amplitude of Coles's wake function. Since there is slip along the centerline of such a recirculating base flow, these profiles cannot be used to develop a correlation for c_f. In view of the characteristically small values of c_f in the laminar part of the bubble, however, it still seems worthwhile to investigate the correlations for the shape factors and C_D and compare them to those obtained with the Stewartson profiles.

By applying the definitions for the integral thicknesses of the boundary layer and for the dissipation coefficient, the following relationships are obtained:

$$H_{12} = \frac{1 + 2\frac{h}{b}}{(1 - \frac{3}{2}G) - 2\frac{h}{b}(1 - 2G)} \tag{17}$$

$$H_{32} = \frac{(2 - \frac{9}{2}G + \frac{5}{2}G^2) + 4\frac{h}{b}(1 - 3G + 2G^2)}{(1 - \frac{3}{2}G) - 2\frac{h}{b}(1 - 2G)} \tag{18}$$

$$R_{\delta_2} C_D = \frac{\pi^2 G^3}{2}[1 - \frac{3}{2}G + 2\frac{h}{b}(1 - 2G)] \tag{19}$$

In order to compare these relationships to those obtained from the Stewartson profiles, it is necessary to know how the two parameters vary inside the bubble. The values used by

Fitzgerald and Mueller to fit the profiles measured inside one bubble can serve as a starting point. The three boundary-layer variables are evaluated at values of the parameters corresponding to the same downstream station inside the bubble and then plotted against each other. The same calculations are then repeated for values G and (h/b) similar to those used in Ref. 5 in order to determine the sensitivity of the correlations to these parameters. The result is shown in Figs. 21 and 22 where these new two-parameter correlations are compared to those developed by Drela from the Stewartson profiles. The solid lines utilize the fitted variations of G and (h/b). As both H_{12} and H_{32} increase monotonically between separation and transition, moving to greater values of the abscissa on these plots corresponds to moving downstream inside the bubble. Thus, both are very similar to the Stewartson correlations near separation but can be quite different further downstream.

The new correlations are very encouraging. While $H_{12}(H_{32})$ seems quite sensitive to changes in the parameters, $C_D(H_{32}, R_{\delta_2})$ is not, thereby making the determination of its exact dependence on G and (h/b) less crucial. It appears from the measurements that the back-flow, proportional to G, may be constant within each bubble although different for different bubbles. As shown in Fig. 21, the values of shape factors actually measured, although different in absolute value, follow the same slope, thus confirming a constant value of back-flow velocity. These considerations justify eliminating (h/b) between Eqs. 17 and 18 and expressing the closure relationships in terms of H_{32}, calculated from the governing equations and G, whose behavior within each bubble appears easier to correlate to local flow conditions,

$$H_{12} = \frac{3(1-G) - H_{32}}{(1-G)(1-2G)} \tag{20}$$

$$R_{\delta_2} C_D = \frac{\pi^2 G^3}{2} \left[1 - \frac{3}{2} G - \frac{(4-5G)(1-G) - (2-3G)H_{32}}{4(1-G) - 2H_{32}} \right] \tag{21}$$

Thus, the unknown parts of the boundary-layer method for the laminar part of the bubble have been reduced to G and c_f. Physically grounded assumptions can be made about variational trends for both variables, however. For instance, it is reasonable to expect that, as the pressure gradient along the bubble increases, the strength of the recirculating

flow, and therefore G, increases also. With increasing back-flow, c_f becomes more negative. Although a precise knowledge of the function $c_f(H_{32}, G, R_{\delta_2})$ is lacking, an approximation will suffice to test whether P, or a suitable alternative, can close the boundary-layer method by serving as independent parameter for both DU and G.

The introduction of an additional parameter defining the velocity profiles leads to a much more complex transition criterion than presently employed. Any one of the n-contours in Fig. 13 shows the variation of the stability characteristics of the Stewartson profiles with changes in the single parameter H_{12}. Here H_{12} is a unique function of the pressure gradient parameter appearing in the Falkner-Skan equation and defining the Falkner-Skan profiles. If an additional parameter defining a family of velocity profiles is added, as is the case with Green's profiles, then a linear stability analysis will yield a family of n-contours for *each* value of n. Each member of this constant-n family of contours corresponds to a different value of the *second* parameter defining the velocity profiles. In physical terms, this means that the velocity profiles will become more unstable as the free shear layer detaches itself from the airfoil surface and as the amount of back-flow increases. Therefore, for a value of $n = 9$, for instance, each contour should follow the behavior Eq. (16) as (h/b), or H_{32}, increases and a separate transition criterion will be necessary for each different value of G. This issue is currently being addressed.

Another important factor affecting the behavior of separation bubbles is the level of the freestream turbulence intensity. Although small in flight, this can have a strong influence on wind-tunnel tests. Therefore, properly accounting for it becomes indispensible for the development of a useful bubble model. In addition, many aerodynamic vehicles do not have smooth surfaces or may suffer from insect contamination. The present version of the Eppler and Somers code lumps both effects into a parameter which controls the position of the transition locus on the boundary-layer development plot. The present configuration of the bubble model makes the extension of this treatment of roughness/freestream turbulence straightforward. After the development of the bubble model has been completed and its generality and accuracy in low-turbulence flow over smooth surfaces have been assessed,

its range of application will be extended to take into account roughness and freestream turbulence.

IV. REFERENCES

1. Gaster, M., "The Structure and Behaviour of Separation Bubbles," Aeronautical Research Council R. & M. No. 3595, March 1967.

2. Eppler, R., and Somers, D. M., "A Computer Program for the Design and Analysis of Low-Speed Airfoils," NASA TM-80210, 1980.

3. Stewartson, K., "Further Solutions of the Falkner-Skan Equation," *Proceedings of the Cambridge Philosophical Society*, vol. 50, 1954, pp. 454-465.

4. Green, J. E., "Two-Dimensional Turbulent Reattachment as a Boundary-Layer Problem," *Separated Flows*, AGARD Conference Proceedings No. 4, Part 1, May 1966.

5. Fitzgerald, E. J., and Mueller, T. J., "Laser Doppler Velocimeter measurements of the Transitional Separation Bubble on an Airfoil at a Low Reynolds Number," submitted to the *AIAA Journal.*

6. Maughmer, M., "A Computationally Efficient Modelling of Laminar Separation Bubbles," NASA CR-182417, February 1988.

7. Horton, H. P., "A Semi-empirical Theory for the Growth and Bursting of Laminar Separation Bubbles," Aeronautical Research Council C. P. 1073, June 1967.

8. Roberts, W. B., "Calculation of Laminar Separation Bubbles and Their Effects on Airfoil Performance," AIAA Paper 79-0285, January 1979.

9. McGhee, R. J., Walker, B. S., and Millard, B. F., "Experimental Results for the Eppler 387 Airfoil at Low Reynolds Numbers in the Langley Low-Turbulence Pressure Tunnel," NASA TM-4062, October 1988.

10. Schmidt, G. S., "The Prediction of Transitional Separation Bubbles at Low Reynolds Numbers," Ph.D. Thesis, Department of Aerospace and Mechanical Engineering, University of Notre Dame, December 1986.

11. Ingen, J. L. van, "On the Calculation of Laminar Separation Bubbles in Two-Dimensional Incompressible Flow," *Flow Separation*, AGARD Conference Proceedings No. 168, 1975.

12. Ingen, J. L. van and Boermans, L. M. M., "Aerodynamics at Low Reynolds Numbers: A Review of Theoretical and Experimental Research at Delft University of Technology," *Conference on Aerodynamics at Low Reynolds Numbers* $10^4 < R < 10^6$, vol. I, Royal Aeronautical Society (London), October 1986, pp. 1.1-1.40.

13. O'Meara, M. M., and Mueller, T. J., "Experimental Determination of the Laminar Separation Bubble Characteristics of an Airfoil at Low Reynolds Numbers," AIAA Paper 86-1065, May 1986.

14. Felsch, K. O., Geropp, D., and Waltz, A., "Method for Turbulent Boundary Layer Prediction," *Proceedings of the Stanford Conference on the Computation of Turbulent Boundary Layers*, vol. 1, 1968, pp. 170-176.

15. Miley, S. T., "An Analysis of the Design of Airfoil Sections for Low Reynolds Numbers," Ph.D. Thesis, Mississippi State University, 1972.

16. Eppler, R. "Recent Developments in Boundary Layer Computation," *Conference on Aerodynamics at Low Reynolds Numbers* $10^4 < R < 10^6$, vol. II, Royal Aeronautical Society (London), October 1986, pp. 12.1-12.18.

17. Ingen, J. L. van, "A Suggested Semi-Empirical Method for the Calculation of the Boundary Layer Transition Region," Delft University of Technology, Department of Aerospace Engineering report VTH-74, 1956.

18. Smith, A. M. O., and Gamberoni, N., "Transition, Pressure Gradient, and Stability Theory," Douglas Aircraft Co. report ES 26338,1956.

19. Evangelista, R., and Vemuru, C. S., "Evaluation of an Analysis Method for Low-Speed Airfoils by Comparison with Wind Tunnel Results," AIAA Paper 89-0266, January 1989.

20. Drela, M., "Two-Dimensional Transonic Aerodynamic Design and Analysis using the Euler Equations," Ph.D. Thesis, MIT, 1986.

21. Brendel, M., and Mueller, T. J., "Boundary Layer Measurements on an Airfoil at Low Reynolds Numbers," *Journal of Aircraft*, Vol. 25, July 1988, pp. 612-617.

22. Bell, W. A., and Cornelius, K. C., "An Experimental Investigation of a Laminar Separation Bubble on a Natural Laminar Flow Airfoil," AIAA Paper 87-0458, January 1987.

23. Hoheisel, H. et al., "A Comparison of Laser-Doppler Anemometry and Probe Measurements within the Boundary Layer of an Airfoil at Subsonic Flow," *Laser Anemometry in Fluid Mechanics - II, Selected Papers from the Second Intl. Symp. on Applications of Laser Anemometry to Fluid Mechanics*, Lisbon, Portugal, July 1984, LADOAN, pp. 143-157.

24. Arnal, D., "Description and Prediction of Transition in Two-Dimensional Incompressible Flow," *Special Course on Stability and Transition of Laminar Flow*, AGARD Report No. 709, March 1984.

25. Eppler, R. "Practical Calculation of Laminar and Turbulent Bled-Off Boundary Layers, NASA TM-75328, 1978. (Translated from *Ingenieur Archiv*, Vol. 32, 1963, pp. 221-245.)

26. Gault, D. E., "An Experimental Investigation of Regions of Separated Laminar Flow," NACA Technical Note 3505, September 1955.

27. Mangalam, S. M., Meyers, J. F., Dagenhart, J. R., and Harvey, W. D., "A Study of Laminar Separation Bubbles in the Concave Region of an Airfoil Using Laser Velocimetry," Second ASME Laser Velocimetry Symposium, Miami, Florida, November 17-21, 1985.

28. Crouch, J. D., and Saric, W. S., "Oscillating Hot-Wire Measurements above an FX63-137 Airfoil," AIAA Paper 86-0012, January 1986.

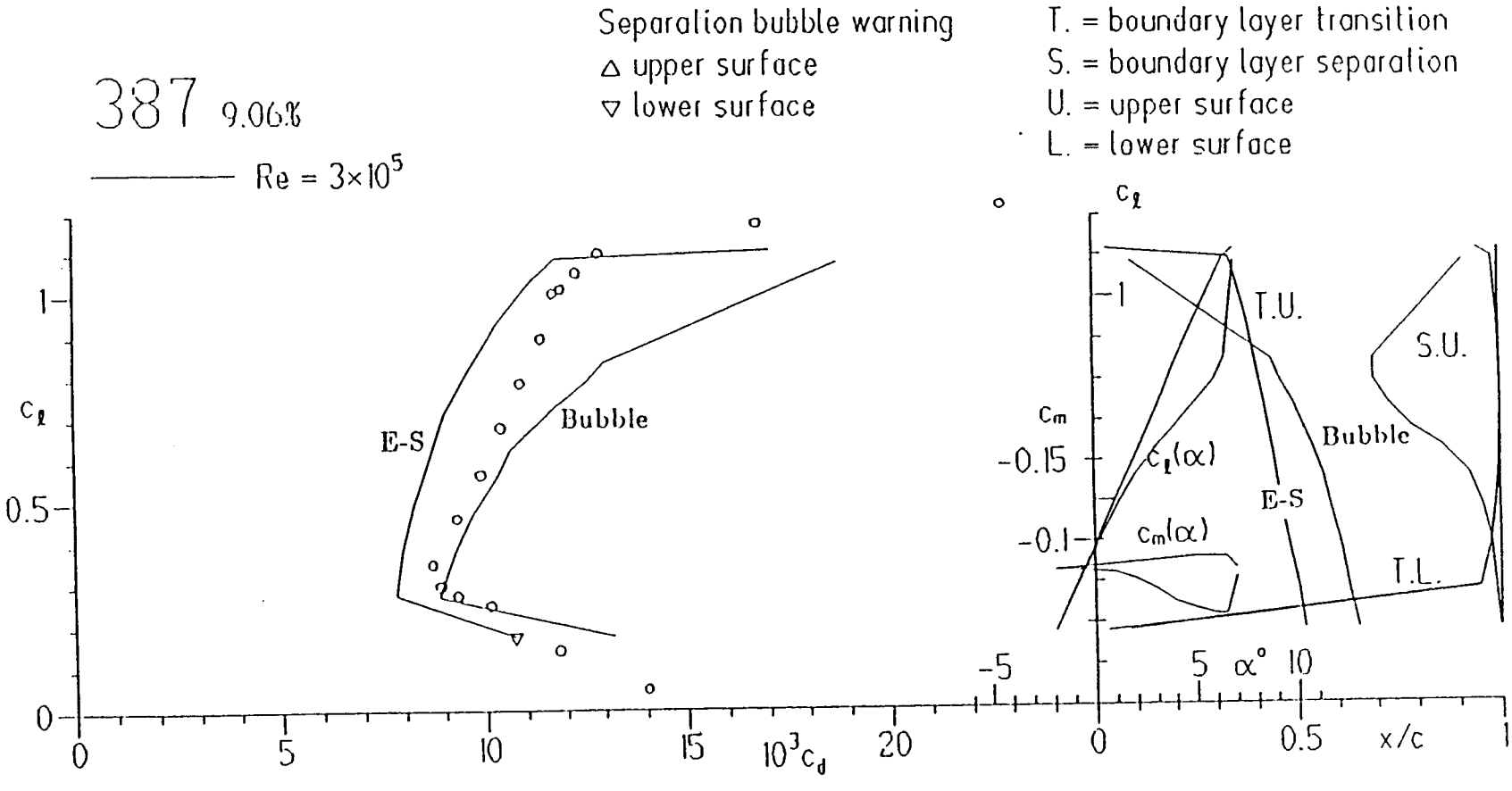

Fig. 1: Aerodynamic characteristics for the Eppler 387 airfoil obtained with the original Eppler and Somers program compared with those obtained using the program incorporating the bubble model with: inviscid C_p, transition, $(\delta_2)_T$ by Schmidt,[10] $U_T = U_S$, Horton's[7] recovery, $(H_{32})_R = 1.51$. Experimental data is from Ref. 9.

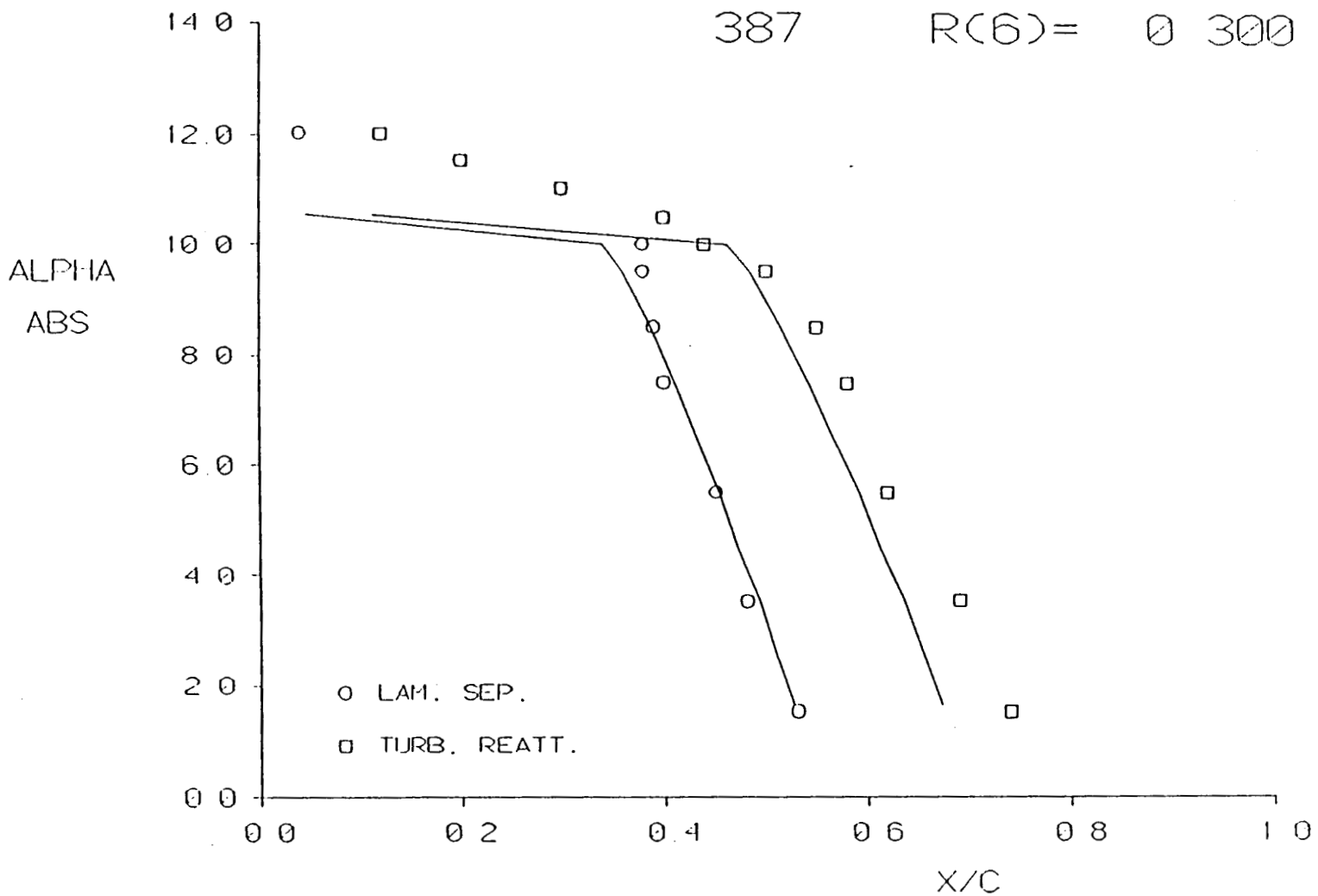

Fig. 2: Comparison of experimental bubble size and location[9] with prediction obtained using the bubble model as described in Fig. 1.

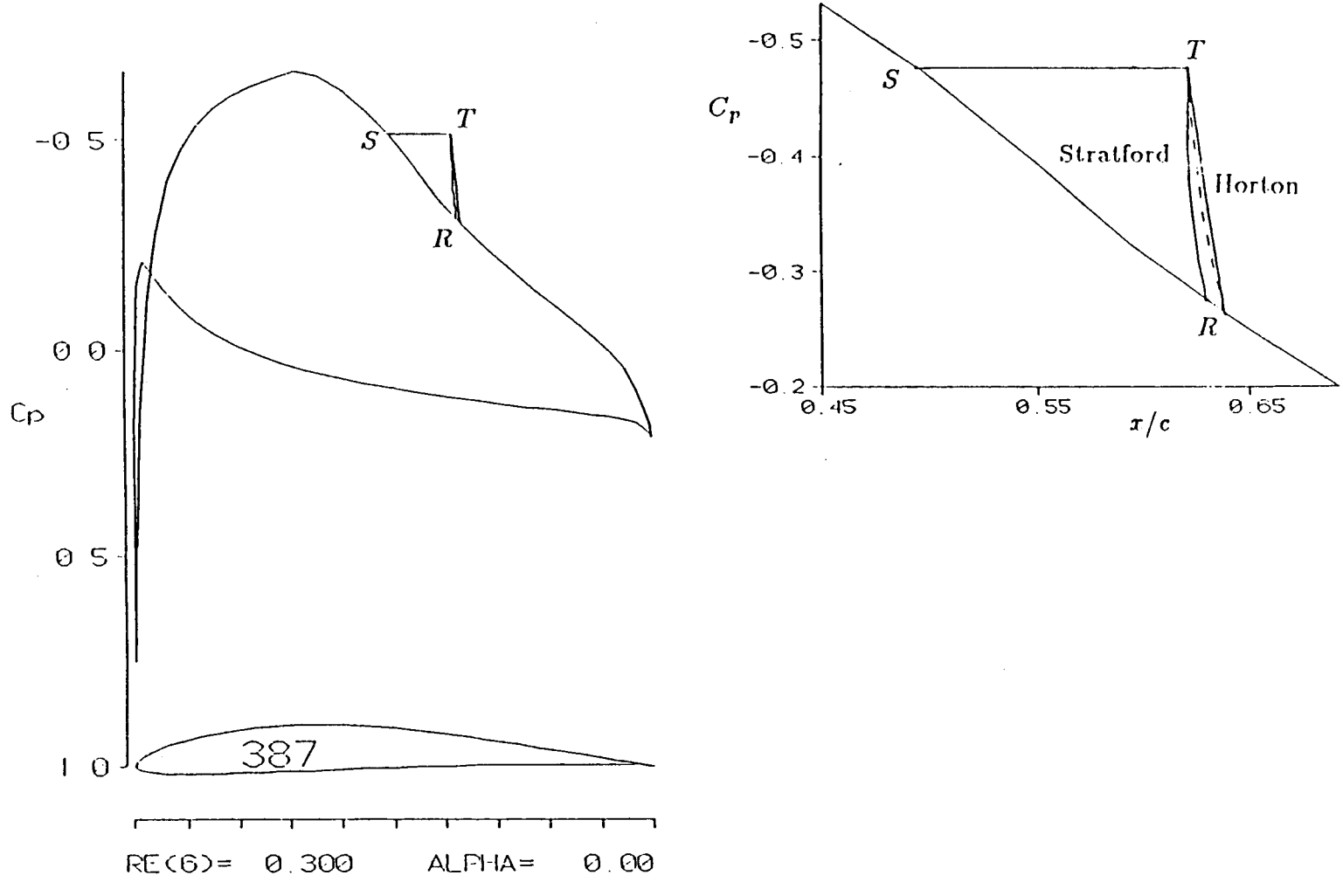

Fig. 3: Comparison of Horton and Stratford recoveries. Inviscid C_p, transition by Schmidt.[10]

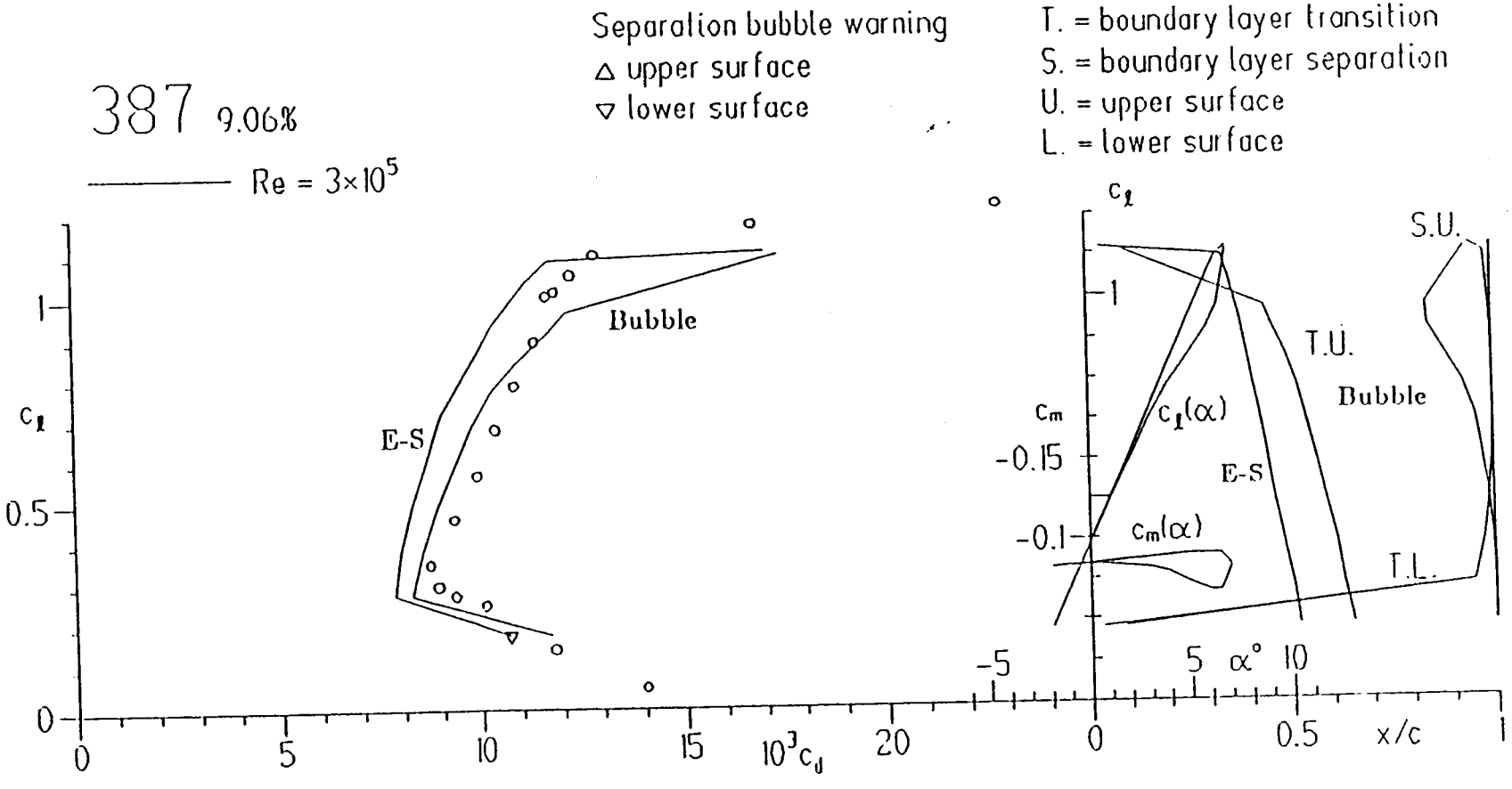

Fig. 4: Aerodynamic characteristics for the Eppler 387 airfoil obtained with the original Eppler and Somers program compared with those obtained using the program incorporating the bubble model with: inviscid C_p, transition, $(\delta_2)_T$ by Schmidt,[10] $U_T = U_S$, Stratford recovery, $(H_{32})_R = 1.51$. Experimental data is from Ref. 9.

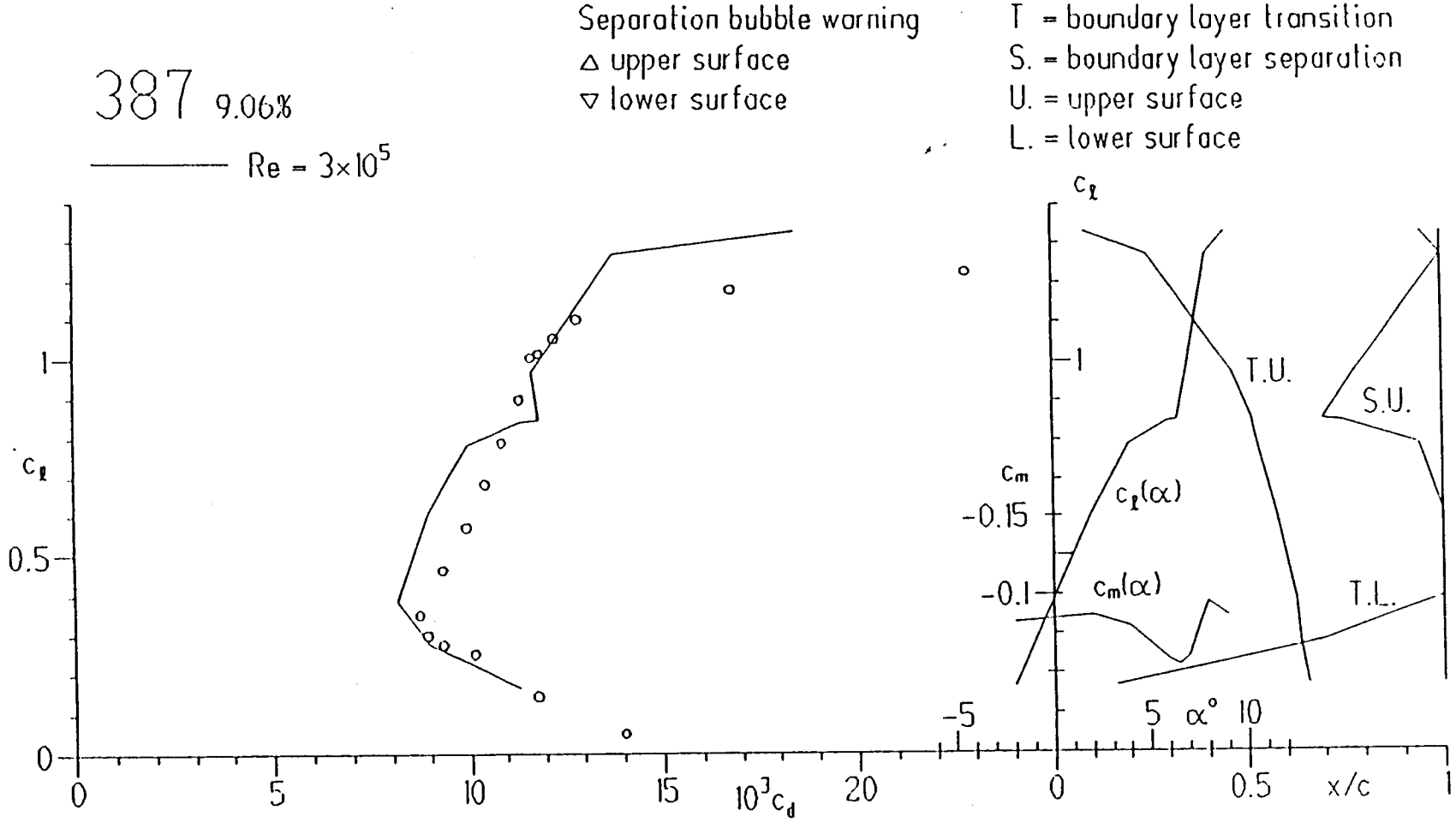

Fig. 5: Aerodynamic characteristics for the Eppler 387 airfoil obtained using the bubble model with: experimental[5] C_p, transition, $(\delta_2)_T$ by Schmidt,[10] $U_T = U_S$, Stratford recovery, $(H_{32})_R = 1.51$. Experimental data is from Ref. 9.

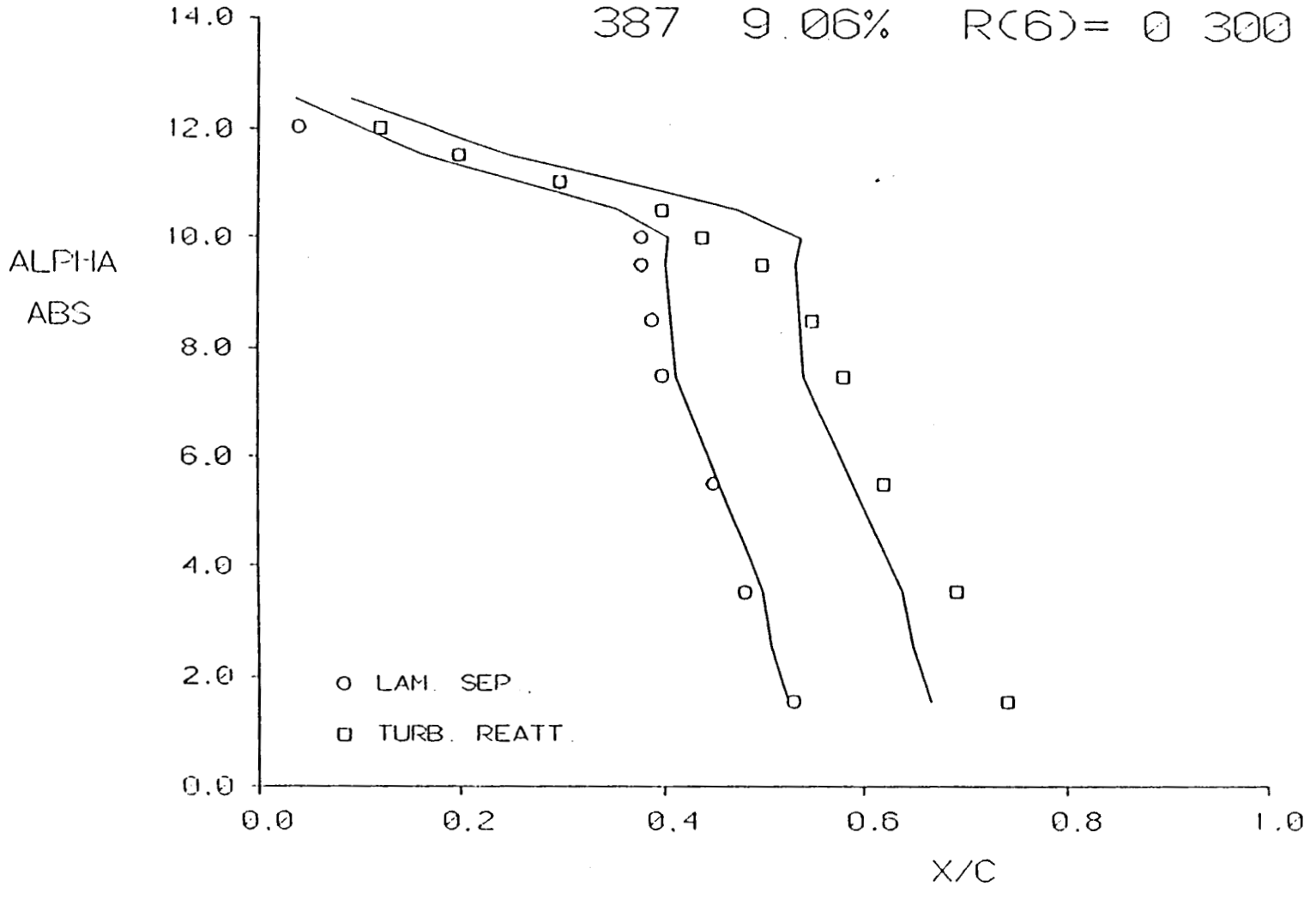

Fig. 6: Comparison of experimental bubble size and location[9] with prediction obtained using the bubble model as described in Fig. 5.

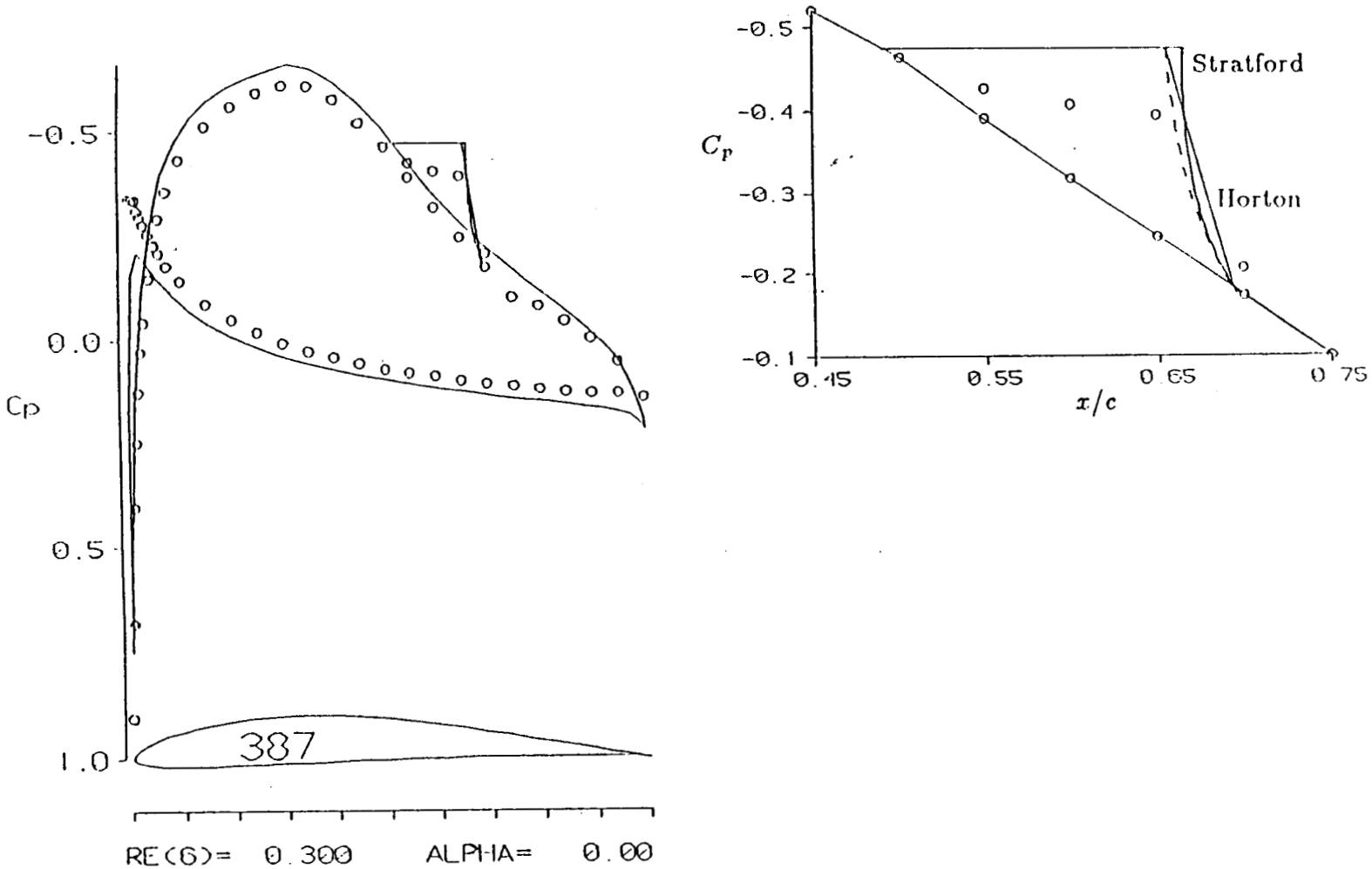

Fig. 7: Comparison of Horton and Stratford recoveries. Experimental C_p, experimental reattachment point.[9]

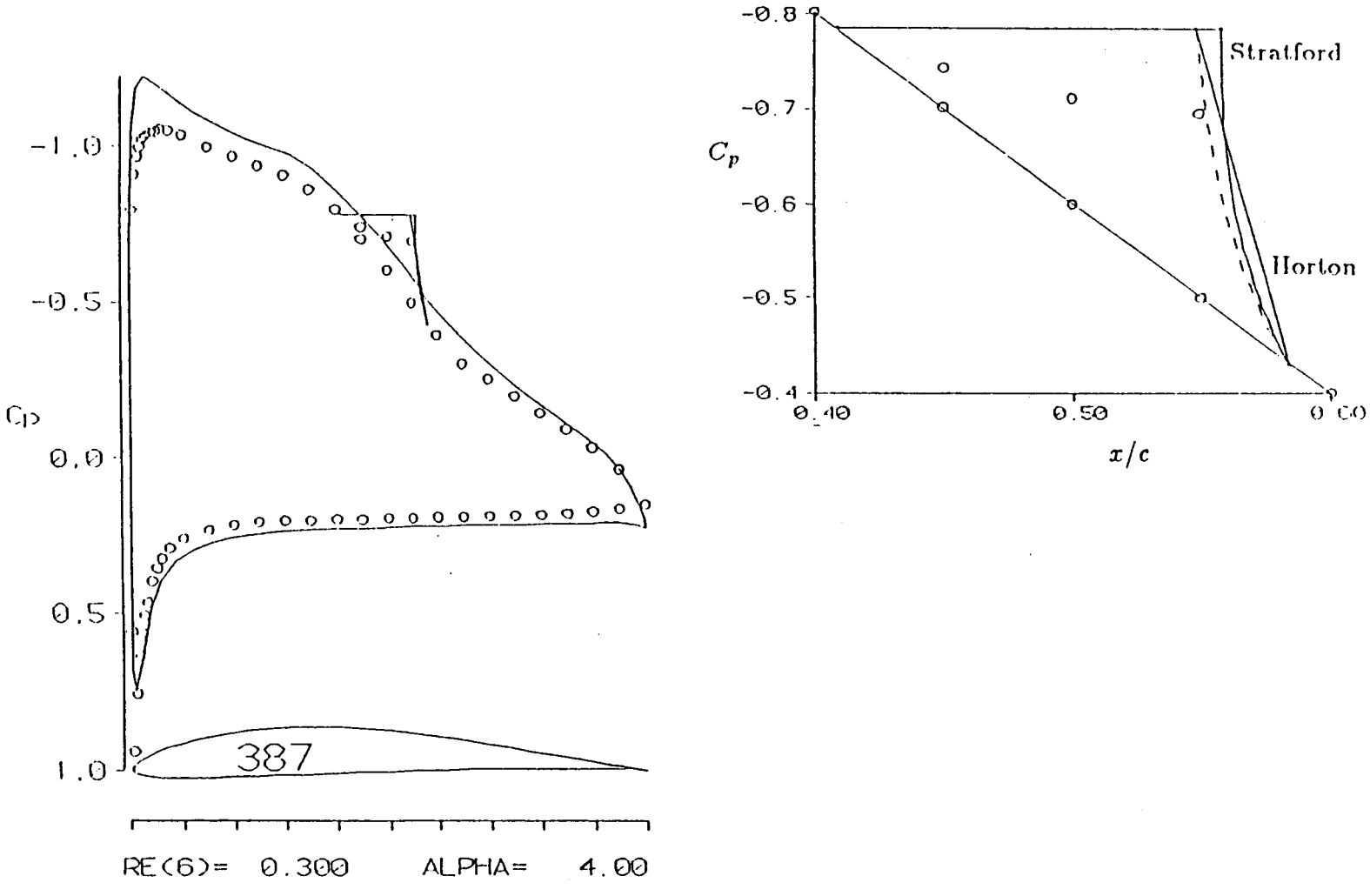

Fig. 8: Comparison of Horton and Stratford recoveries. Experimental C_p, experimental reattachment point.[9]

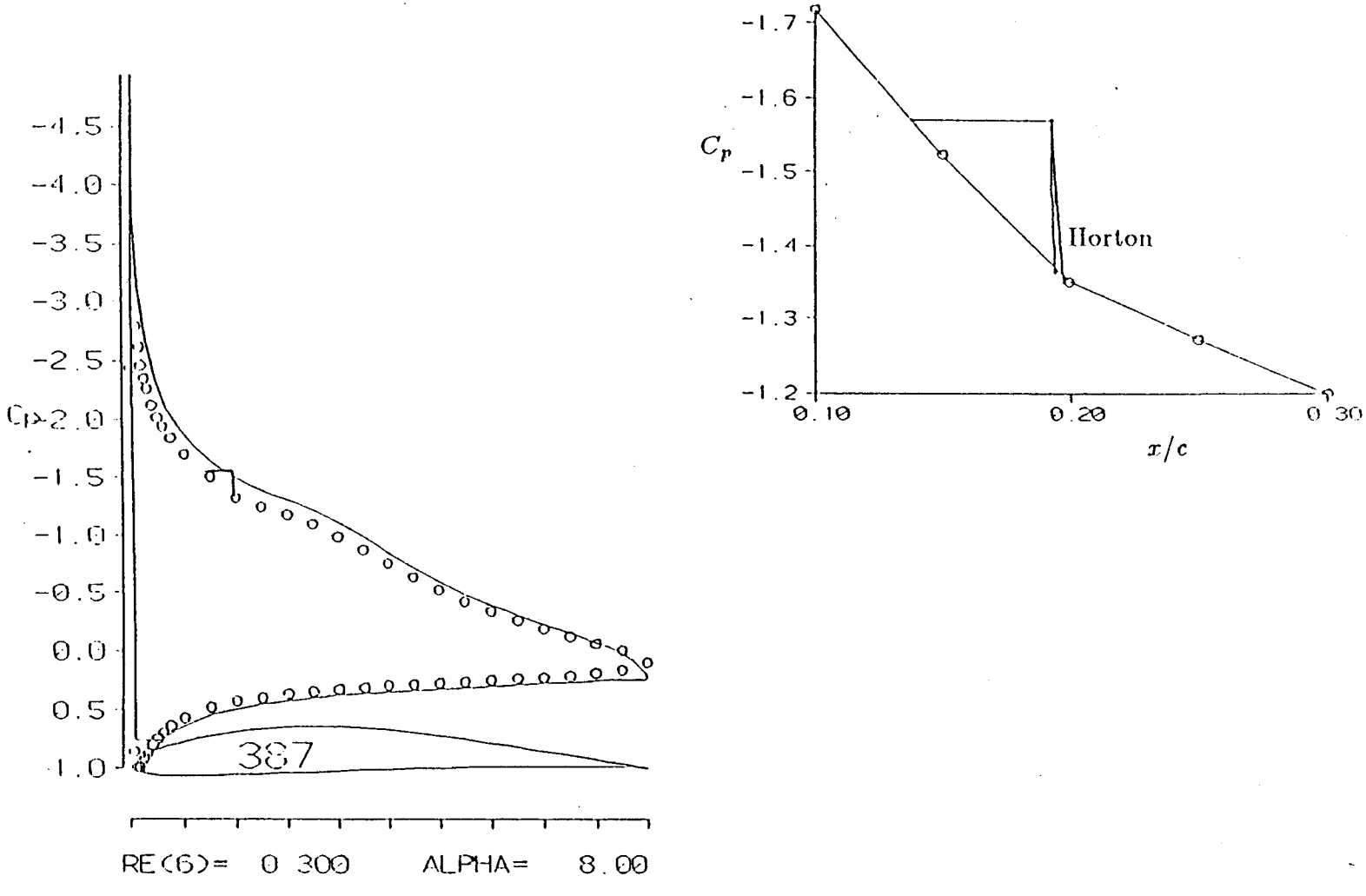

Fig. 9: Comparison of Horton and Stratford recoveries. Experimental C_p, experimental reattachment point.[9]

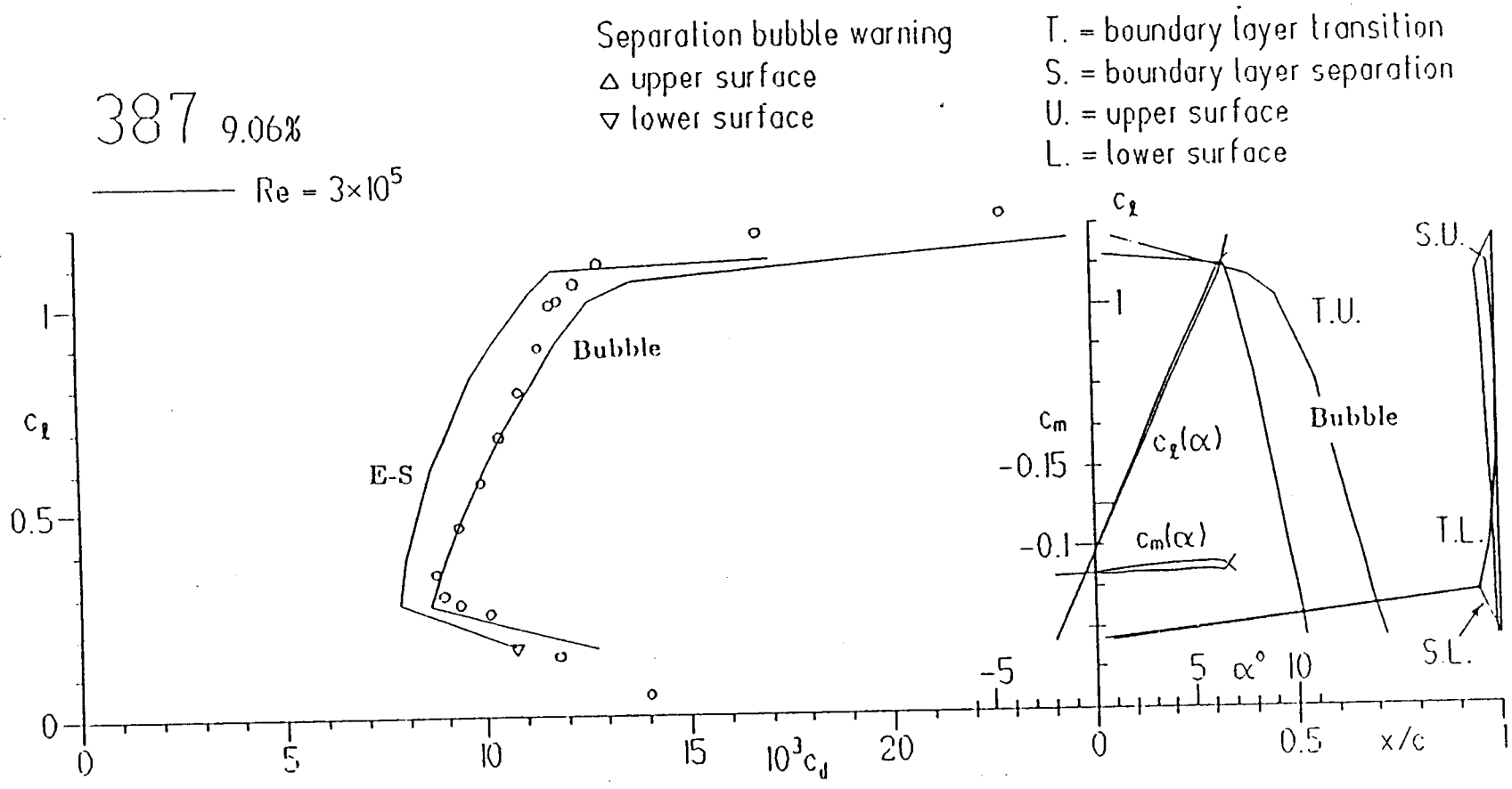

Fig. 10: Aerodynamic characteristics for the Eppler 387 airfoil obtained with the original Eppler and Somers program compared with those obtained using the program incorporating the bubble model with: inviscid C_p, experimental reattachment point,[9] $(\delta_2)_T$ by Schmidt,[10] U_T from Eq. (1), Stratford recovery, $(H_{32})_R = 1.57$. Turbulent boundary-layer method is by Felsch et al.[14]. Experimental data is from Ref. 9.

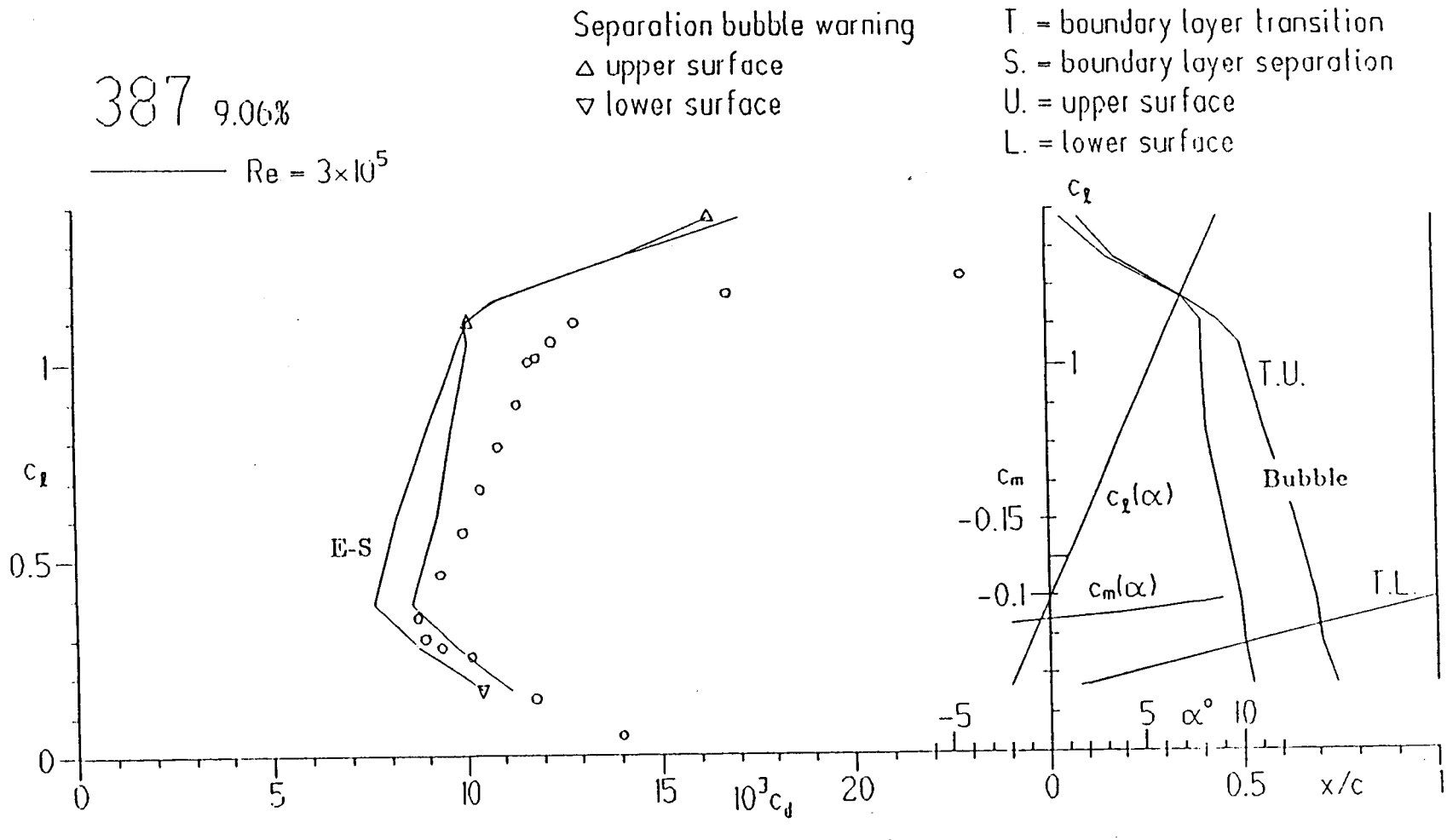

Fig. 11: Aerodynamic characteristics for the Eppler 387 airfoil obtained with the original Eppler and Somers program compared with those obtained using the program incorporating the bubble model with: experimental C_p, experimental reattachment point,[9] $(\delta_2)_T$ by Schmidt,[10] U_T from Eq. (1), Stratford recovery, $(H_{32})_R = 1.57$. Experimental data is from Ref. 9.

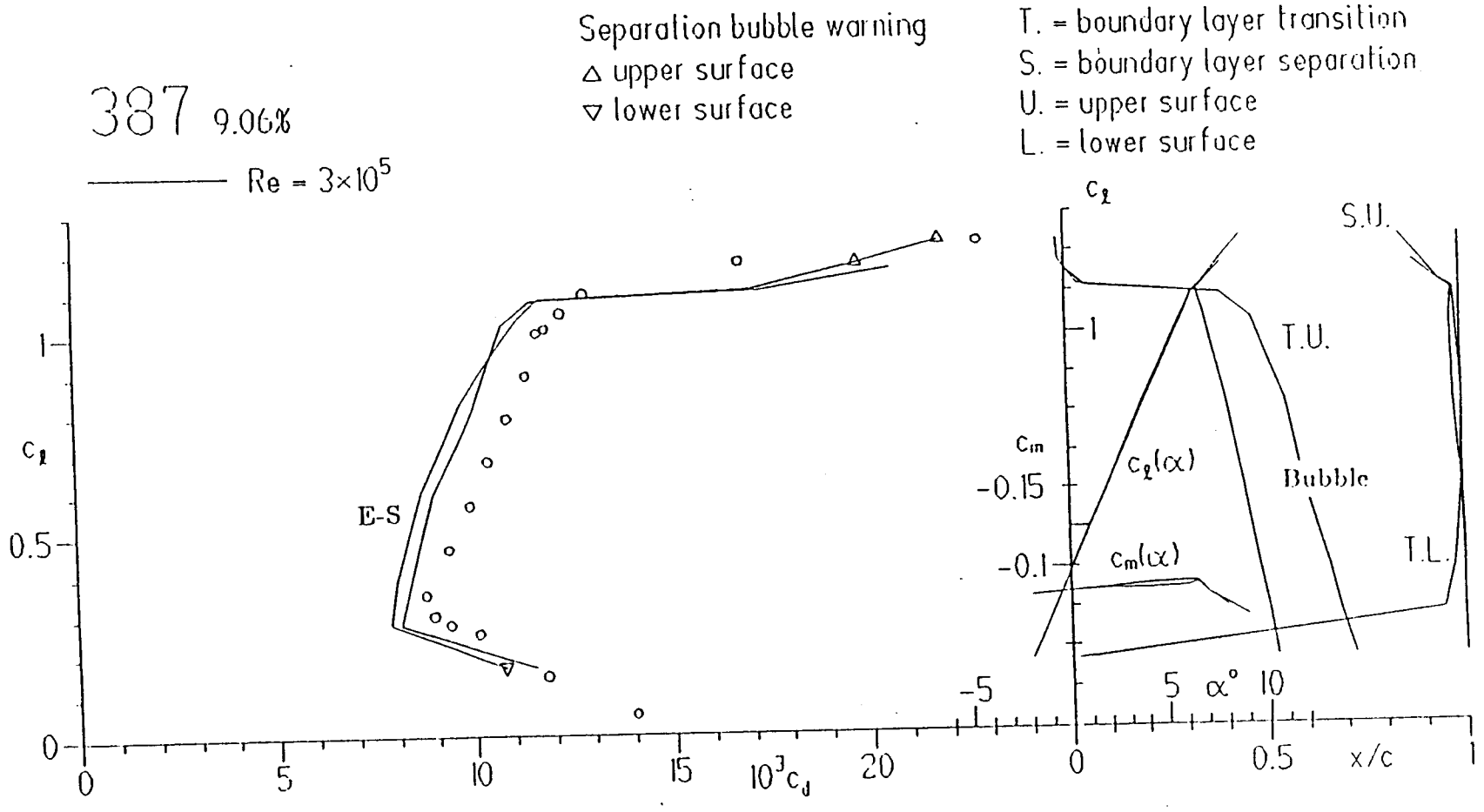

Fig. 12: Aerodynamic characteristics for the Eppler 387 airfoil obtained with the original Eppler and Somers program compared with those obtained using the program incorporating the bubble model with: inviscid C_p, experimental reattachment point,[9] $(\delta_2)_T$ by Schmidt,[10] U_T from Eq. (1), Stratford recovery, $(H_{32})_R = 1.57$. Experimental data is from Ref. 9.

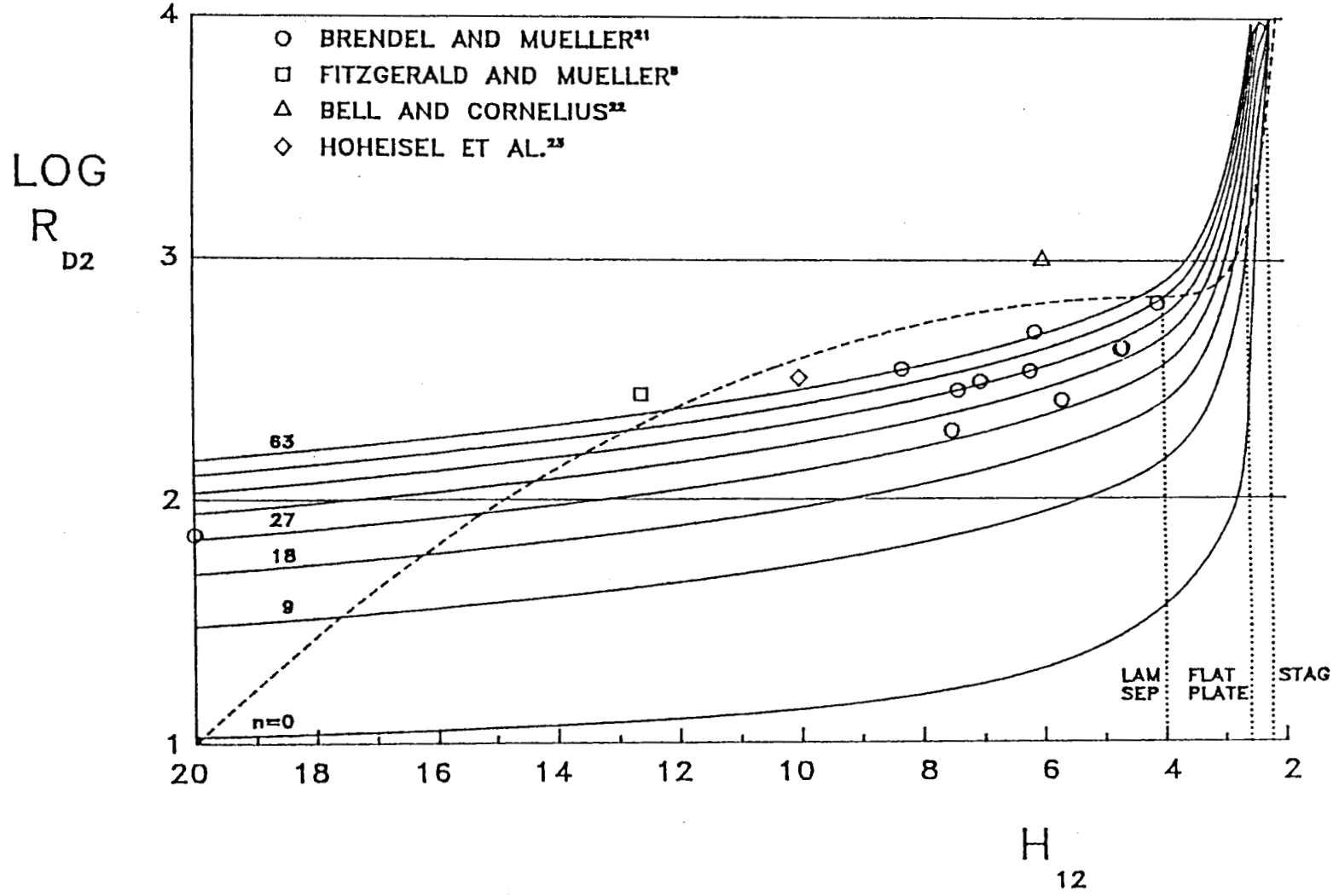

Fig. 13: Comparison of the present transition criterion for separated boundary layers (dashed line, $H_{12} > 4$) with the e^n method[20] and some experimental data. Dashed line, for $H_{12} < 4$, is Eppler's transition criterion for attached boundary layers.

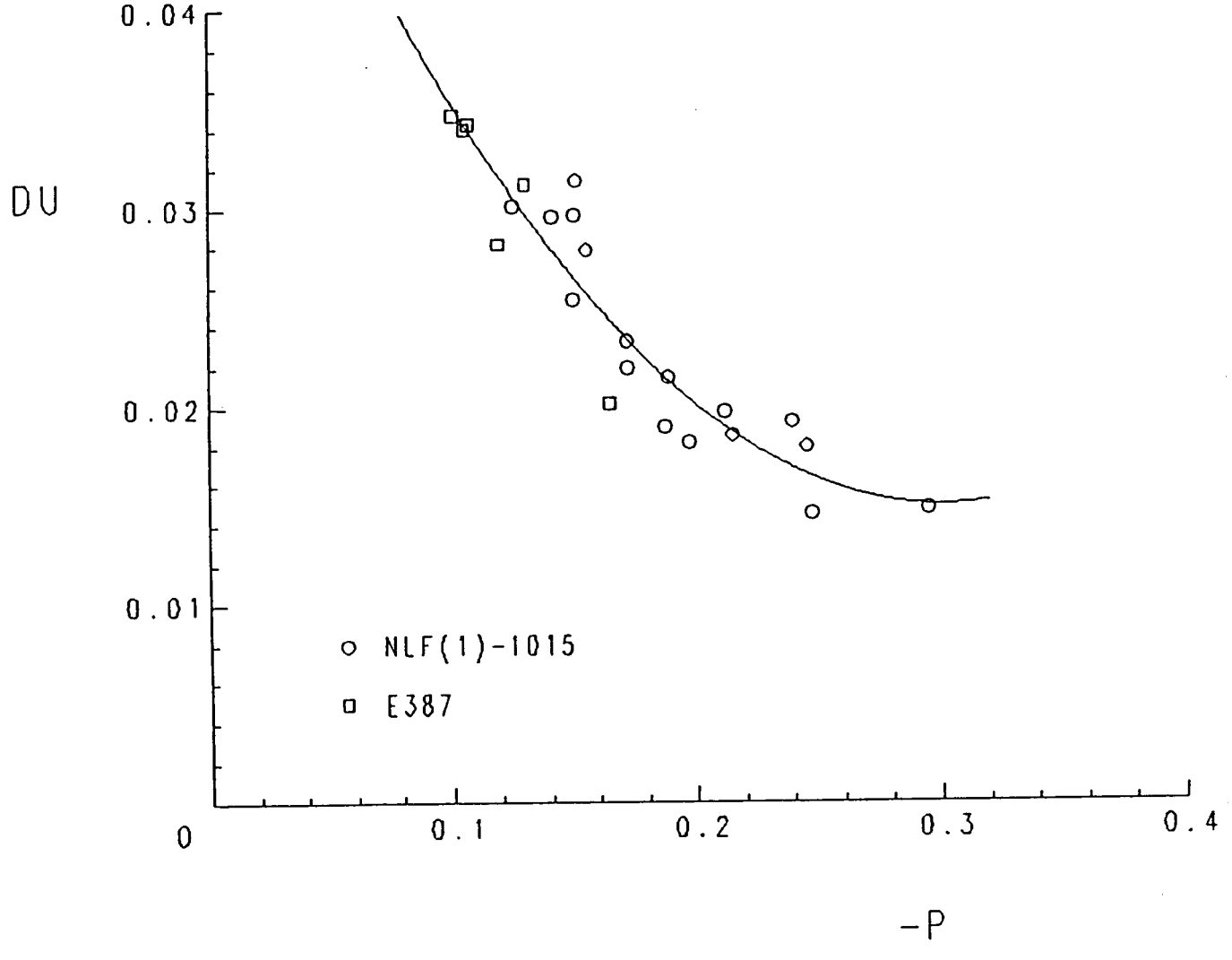

Fig. 14: Pressure recovery in the laminar part of the bubble as a function of Gaster's pressure gradient parameter. ○ : NLF(1)-1015 Airfoil (NASA Langley LTPT, June 1987); □ : E387 Airfoil.[9]

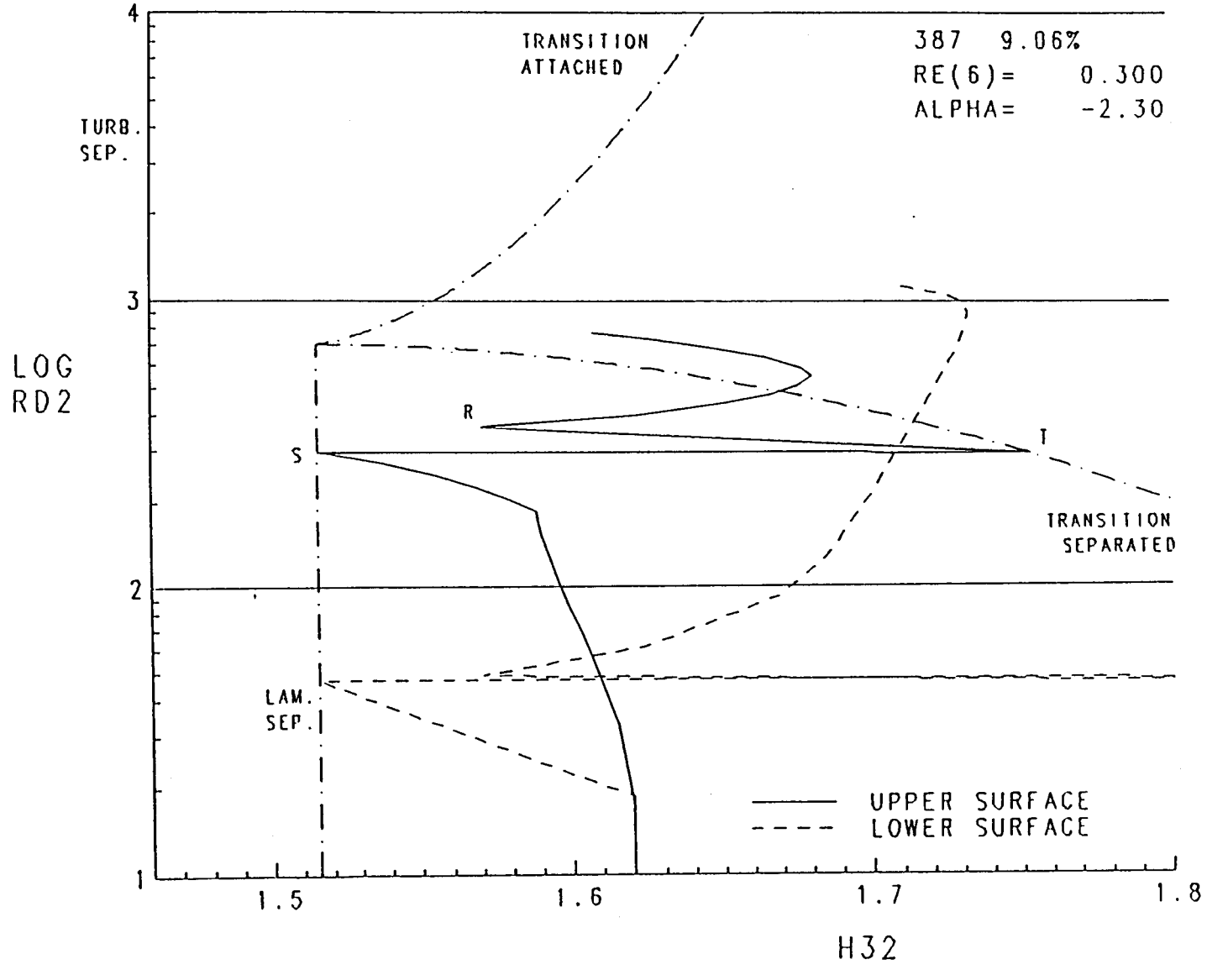

Fig. 15: Modified Eppler's boundary-layer development plot, showing the approximate boundary-layer development inside the bubble.

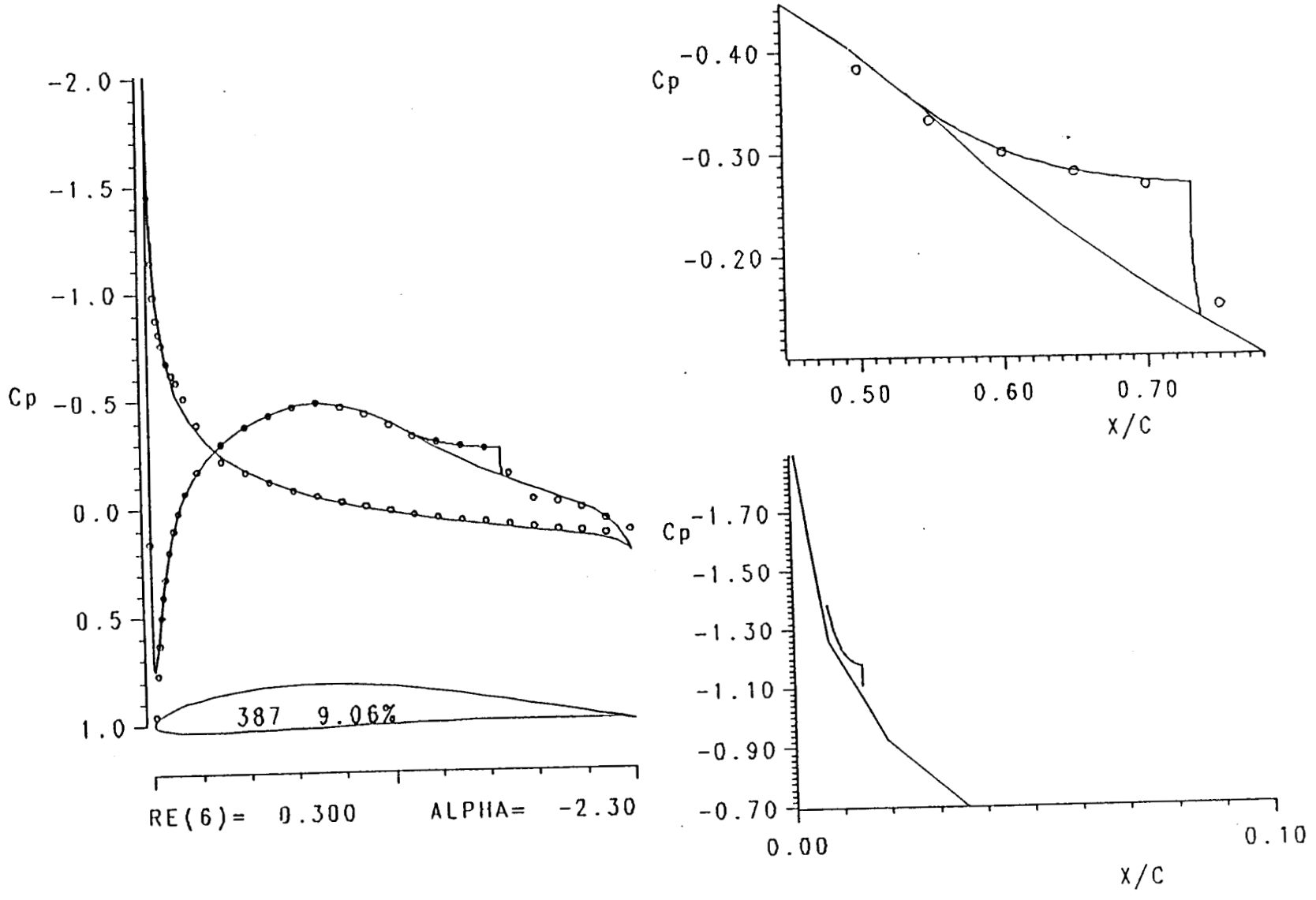

Fig. 16: Comparison of the experimental pressure distribution[9] at $\alpha = -2°$ with the one obtained using the present bubble model at $\alpha = -2.3°$ for the Eppler 387 airfoil.

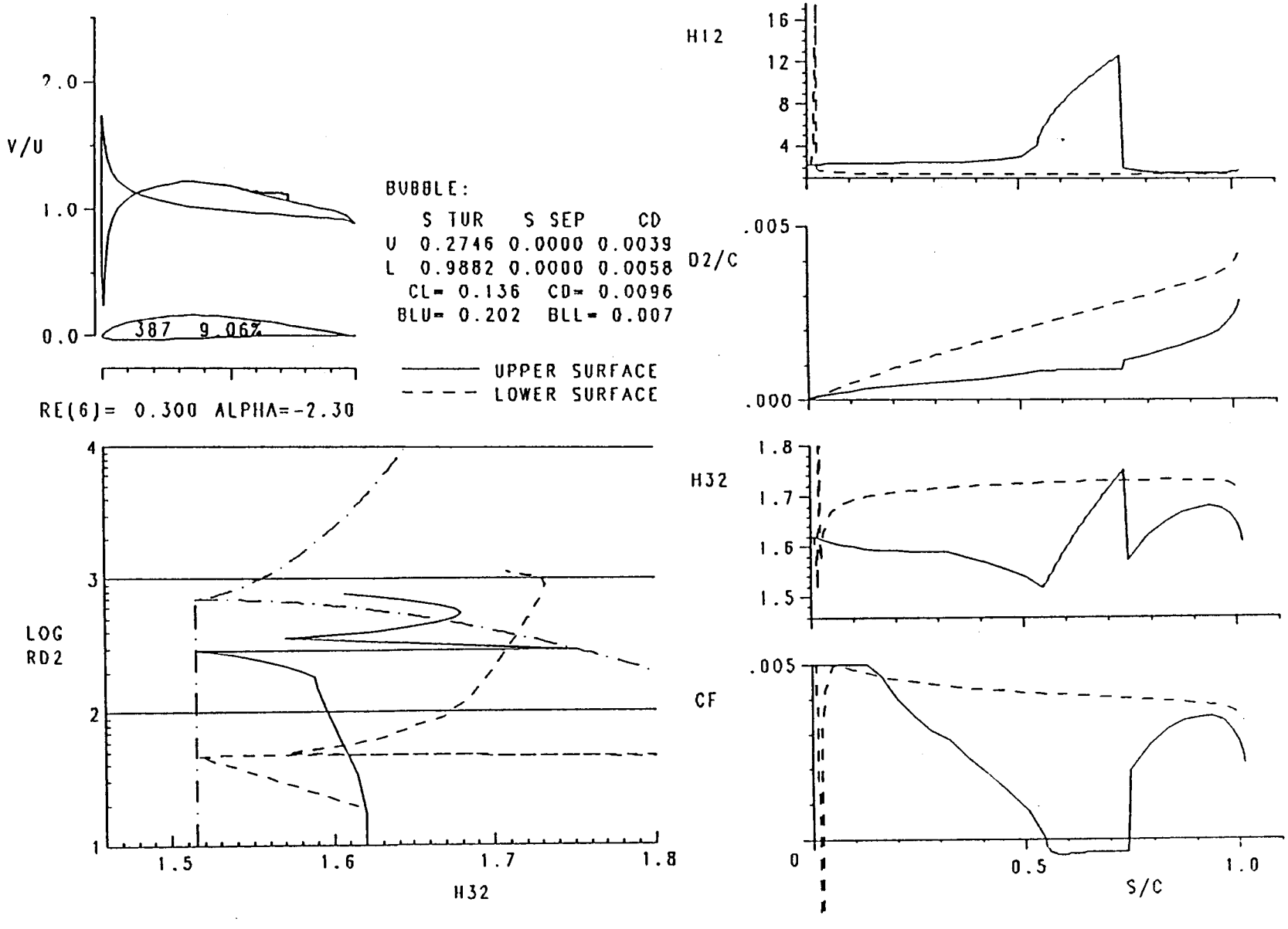

Fig. 17: Viscous analysis summary, details of the boundary-layer development and inviscid velocity distribution for the Eppler 387 airfoil obtained using the present bubble model.

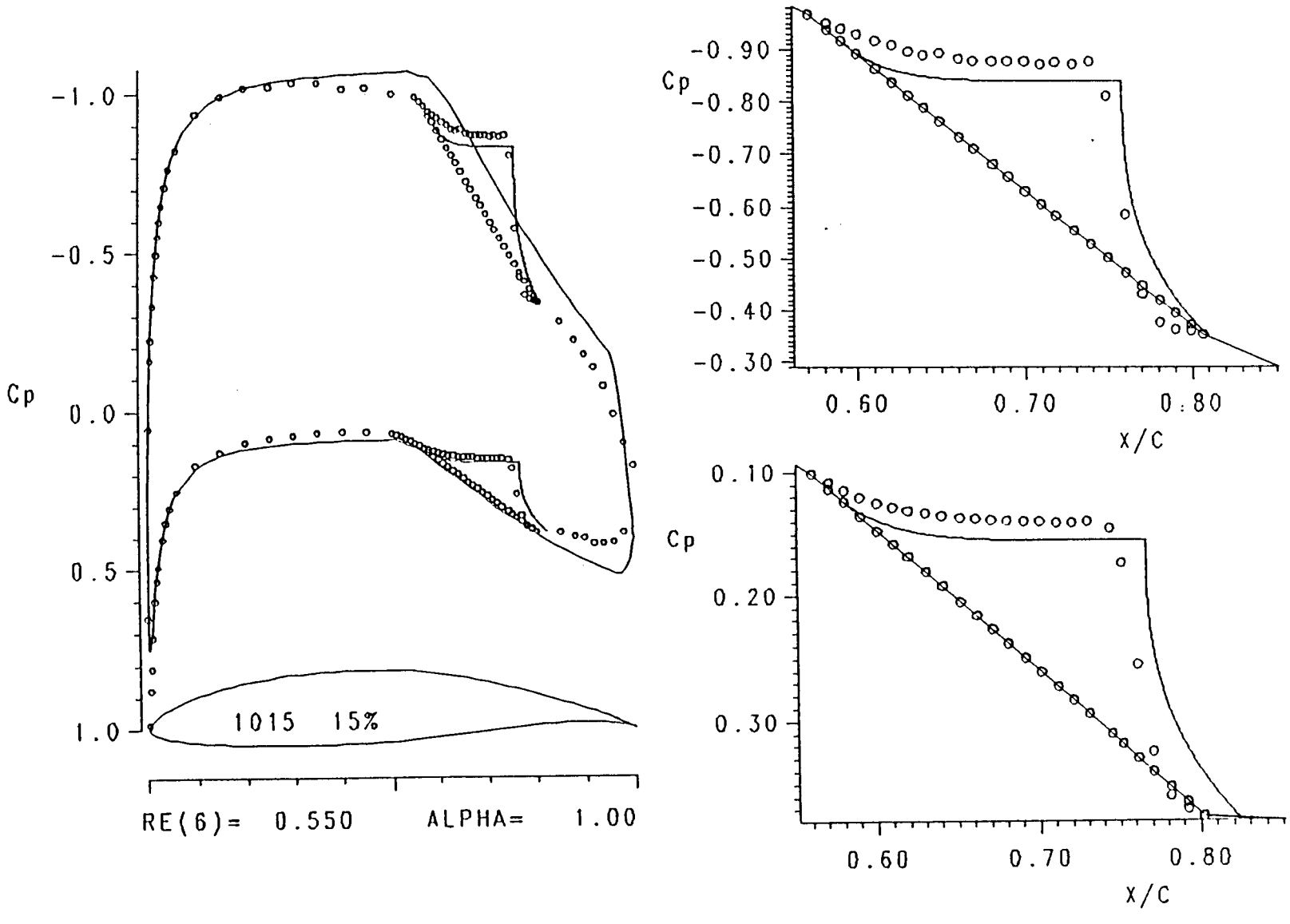

Fig. 18: Comparison of the experimental pressure distribution (NASA Langley LTPT, June 1987) used in conjunction with the present bubble model at $\alpha = 2°$ with the inviscid at $\alpha = 1°$ for the NLF(1)-1015 airfoil.

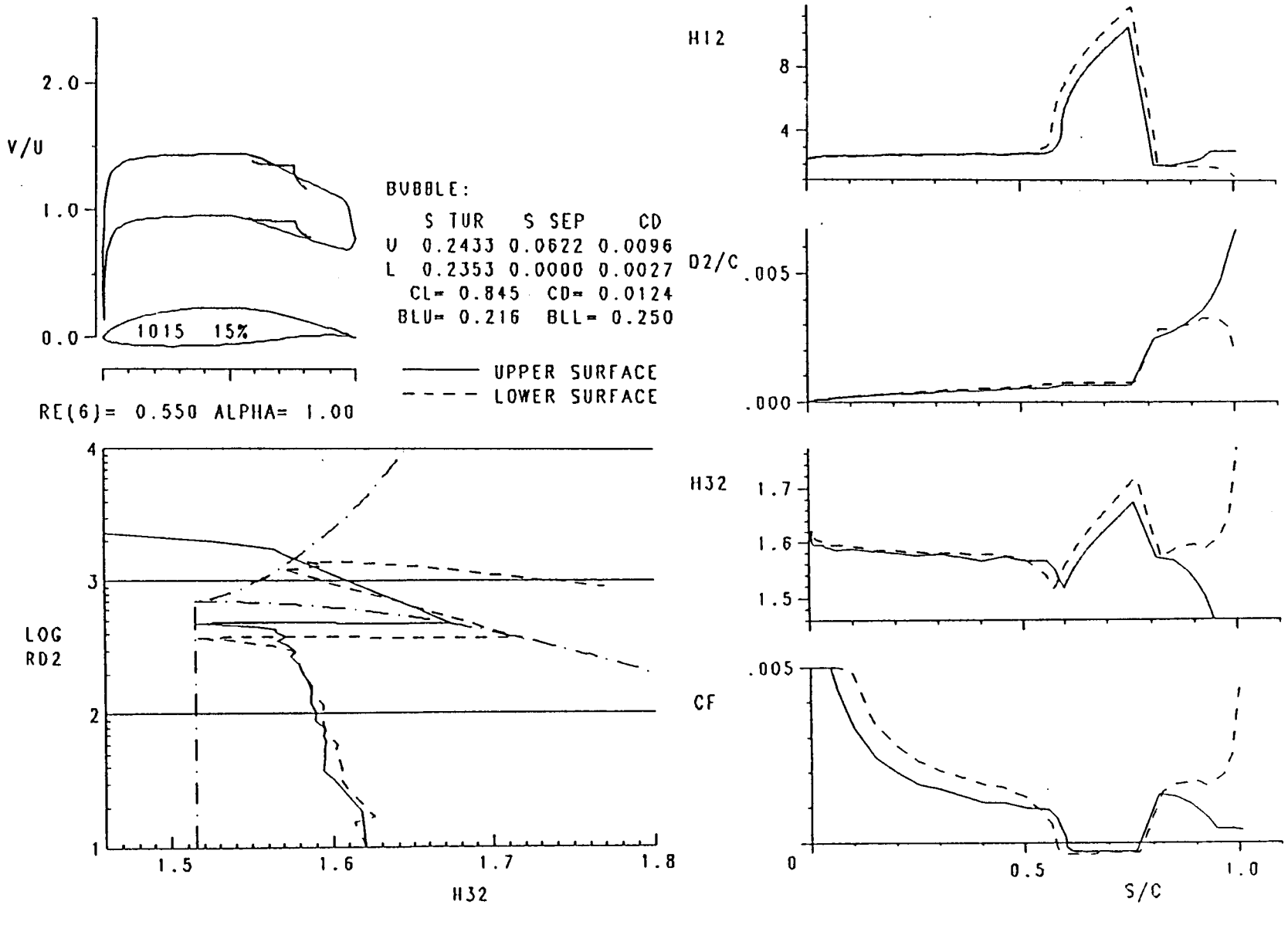

Fig. 19: Viscous analysis summary, details of the boundary-layer development and inviscid velocity distribution for the NLF(1)-1015 airfoil obtained using the present bubble model.

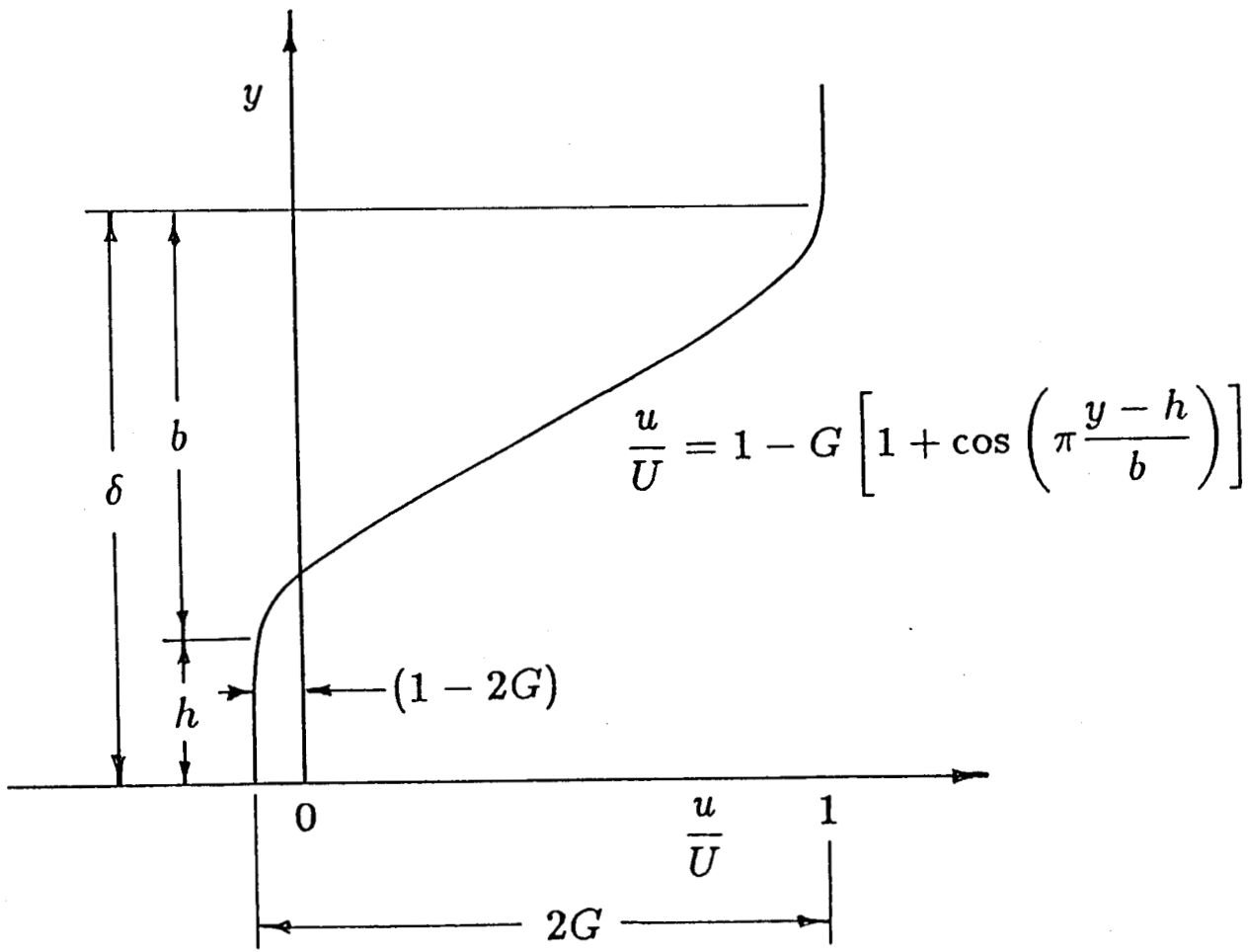

Fig. 20: Two-parameter reversed velocity profile of Green.[4]

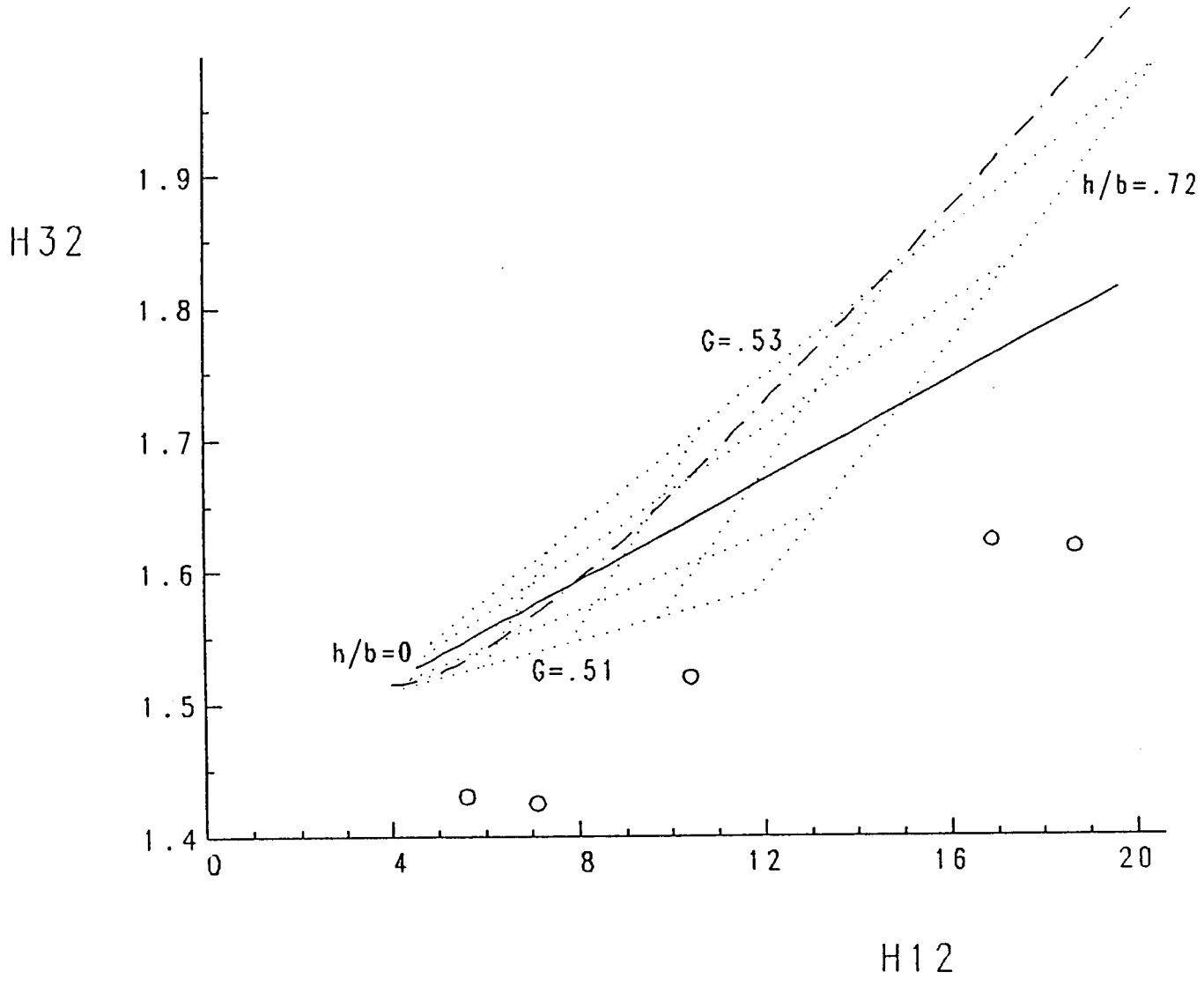

Fig. 21: Comparison of shape factor correlations. —·—·—: Ref. 20, from Stewartson profiles; ———: Ref. 5, from fitted Green's profiles; ·····: Eqs. (17) and (18); ○ : measured, Ref. 5.

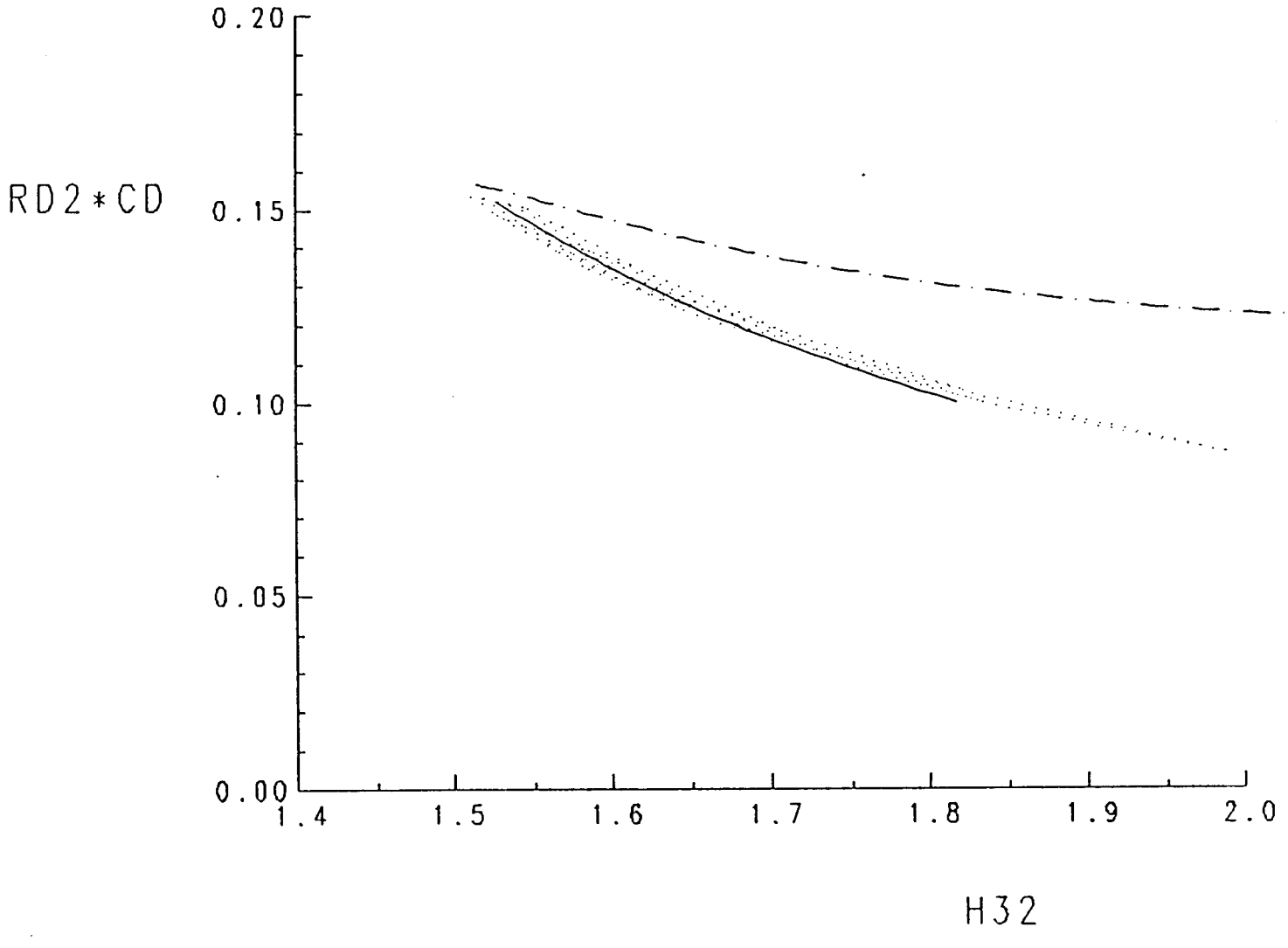

Fig. 22: Comparison of dissipation coefficient correlations. —·—·—: Ref. 20, from Stewartson profiles; ——— : Ref. 5, from fitted Green's profiles; ····· : Eqs. (18) and (19).